Acoustic boundary conditions at an impedance lining in inviscid shear flow

Doran Khamis[1] **and Edward James Brambley**[1],†

[1]Department of Applied Mathematics and Theoretical Physics, University of Cambridge,
Wilberforce Road, Cambridge CB3 0WA, UK

The accuracy of existing impedance boundary conditions is investigated, and new impedance boundary conditions are derived, for lined ducts with inviscid shear flow. The accuracy of the Ingard–Myers boundary condition is found to be poor. Matched asymptotic expansions are used to derive a boundary condition accurate to second order in the boundary layer thickness, which shows substantially increased accuracy for thin boundary layers when compared with both the Ingard–Myers boundary condition and its recent first-order correction. Closed-form approximate boundary conditions are also derived using a single Runge–Kutta step to solve an impedance Ricatti equation, leading to a boundary condition that performs reasonably even for thicker boundary layers. Surface modes and temporal stability are also investigated.

Key words: acoustics, aeroacoustics, boundary layers

1. Introduction

The work of Ingard (1959) and Myers (1980) on the acoustic boundary condition at an impedance surface in a non-quiescent fluid has formed the basis for most subsequent work, industrial and academic (e.g. Tester 1973*b*; Koch & Moehring 1983), where sound attenuation in a moving fluid was important. Over thirty years after the publication of Myers' paper, and over five years since indisputable evidence was presented, both theoretical (Brambley 2009) and experimental (Renou & Aurégan 2011), of its weaknesses, the Ingard–Myers boundary condition continues to be routinely used in aeroacoustics computations to inform engine design.

Inviscid perturbations to a sheared flow over an acoustic liner are governed by the Pridmore-Brown (1958) equation. Modal solutions to this equation show that acoustic liners not only attenuate acoustic modes but also support surface waves – vibrations of the liner and boundary layer – that are not present in the hard-wall case. These waves were classified as surface modes by Rienstra (2003), who used uniform flow and the Myers (or Ingard–Myers) model of the impedance lining to find a possible four surface modes per frequency and circumferential order. This work was extended by Brambley (2013), who accounted for the thin, but non-zero thickness, boundary layer by using the first-order correction terms to the Myers condition (Brambley 2011*b*) and

† Email address for correspondence: e.j.brambley@damtp.cam.ac.uk

found the number of possible surface waves increased to six. At present, no further surface wave solutions to the Pridmore-Brown equation have been identified.

The importance of including a finite-thickness shear layer rather than assuming a uniform slipping flow also manifests in the different convective and absolute stability of the two models. Experimental evidence of an instability in flow over an impedance lining has been reported many times (e.g. Aurégan & Leroux 2008; Marx *et al.* 2010). Theoretical predictions of the instability that utilise the Myers model found that in the time domain a numerical instability would grow at the grid scale and swamp any meaningful signal, while in the frequency domain an unstable mode was found with a growth rate unbounded with increasing wavenumber. This was due to the illposedness of the problem of uniform slipping flow over an impedance lining (Brambley 2009). This illposedness is regularised by taking into account a thin but finite-thickness sheared boundary layer, and modified versions of the Myers condition (Myers & Chuang 1984; Joubert 2010; Brambley 2011*b*; Rienstra & Darau 2011), correct to first order in the boundary layer thickness, predict convectively or absolutely unstable modes with bounded growth rates.

The accuracy of the current inviscid models was investigated by Gabard (2013) by considering reflection of acoustic plane waves from an impedance lining in shear flow. It was found that use of the Myers condition can lead to significant errors (of up to 14 dB) in predictions of sound attenuation due to the great impact of the boundary layer thickness. Modelling the physics inside the boundary layer more precisely, for instance by expanding to second order in the boundary layer thickness, should therefore lead to more accurate predictions of the absorption and reflection coefficients for an acoustic liner in flow. The accuracy of current boundary conditions and the newly derived conditions are tested in a different way here: by comparing with the exact effective impedance found by numerical solution of the Pridmore-Brown equation; and by comparing the prediction of cut-on and cut-off acoustic modes.

There are a number of common simplifications used in the literature that we follow here, since reasonable agreement is possible between theory using these assumptions and practice (e.g. Boyer, Piot & Brazier 2011). Commonly, acoustic liners are manufactured using a perforated facing sheet having hole diameters and spacings of the order of or larger than a typical boundary layer thickness. The majority of the acoustic lining literature models such linings as homogeneous, however, and here we follow this simplification. When applied in shear flow, the Pridmore-Brown equation possesses a singularity, called the critical layer, wherever the phase speed of a wave is equal to the base flow velocity (that is, when a wave is perfectly convected). It has been shown that the contribution to the resultant sound field of the critical layer is modest at most (Brambley, Darau & Rienstra 2012). Here we avoid the critical layer in favour of simplicity. Also omitted from the analysis are viscous and nonlinear effects. It has been shown that viscosity alone does not regularise the illposedness of the Myers condition (Brambley 2011*a*), but when coupled with a finite-thickness shear layer the problem becomes well posed and the visco-thermal effects allow the unstable mode to restabilise below a critical wavelength (Khamis & Brambley 2015) – a phenomenon missing from the inviscid theory. It has also been shown that including viscosity in the boundary layer can be necessary to accurately match theoretical results with experimental data (Renou & Aurégan 2010, 2011). Nonlinearity with respect to the interaction between sound field, shear flow and liner is beyond the scope of this work.

In this work, new boundary conditions are derived that extend the inviscid theory. In § 2 the governing Pridmore-Brown equations for the acoustic pressure $\tilde{p}$ and velocity $\tilde{v}$

are stated, and an impedance Ricatti equation is derived for $Z(r) = \tilde{p}(r)/\tilde{v}(r)$. Section 3 describes the asymptotic analysis leading to a boundary condition that is correct to second order in the boundary layer thickness. Section 4 solves the impedance equation by a single fourth-order explicit Runge–Kutta step across the boundary layer; and by a second-order, single-step implicit scheme. Expressions are given for the effective impedance at the lining seen by the acoustics in a plug flow (uniform mean flow). In §5, the accuracy of each of these models is compared against the Ingard–Myers boundary condition, its first-order correction and numerical simulations. While the second-order boundary condition performs better for thin boundary layers, the single-step implicit Runge–Kutta scheme retains accuracy for high frequencies and short wavelengths, and for thicker boundary layers, making it a viable substitute for the asymptotic boundary conditions outside their regions of validity. In §6, simplified forms of the conditions are found both for a specific linear shear profile and for the limiting case $k/\omega \gg 1$ satisfied by surface modes. In §7 it is found that the second-order asymptotic condition is extremely accurate when investigating surface modes and their stability, as well as cut-on and cut-off acoustic modes. The second-order condition does, however, support spurious modes far from its region of asymptotic validity.

2. Governing equations

We are concerned with the dynamics of an inviscid compressible perfect gas, for which (with a star denoting a dimensional variable) the governing equations take the form

$$\frac{\partial \rho^*}{\partial t^*} + \nabla^* \cdot (\rho^* \boldsymbol{u}^*) = 0, \quad \rho \frac{\mathrm{D}\boldsymbol{u}^*}{\mathrm{D}t^*} = -\nabla^* p^*, \quad \frac{\mathrm{D}p^*}{\mathrm{D}t^*} = c^{*2} \frac{\mathrm{D}\rho^*}{\mathrm{D}t^*}, \qquad (2.1a\text{-}c)$$

where $\mathrm{D}/\mathrm{D}t^* = \partial/\partial t^* + \boldsymbol{u}^* \cdot \nabla^*$ is the material derivative, $\gamma = c_p^*/c_v^*$ is the ratio of specific heats, and p^*, ρ^* and $\boldsymbol{u}^*$ are the fluid pressure, density and velocity, respectively. Equation (2.1c), relating p^* and ρ^*, is a consequence of the assumption that the specific entropy remains constant for a given fluid particle (Pierce 1994); for a perfect gas, the speed of sound satisfies $c^{*2} = \gamma p^*/\rho^*$. To non-dimensionalise, we imagine a cylindrical duct (x, r, θ) with an uniform base flow at its centreline, and scale length by the duct radius l^*, density by the centreline value ρ_0^*, velocity by the centreline sound speed $c_0^* = \sqrt{\gamma p_0^*/\rho_0^*}$, and pressure by $\rho_0^* c_0^{*2}$. Time is made dimensionless by combining the length and velocity scales, $t^* = l^* t/c_0^*$. In such a scheme, the duct radius is unity, and the centreline main-flow density and pressure take the respective values $\rho_0 = 1$ and $p_0 = 1/\gamma$. The dimensionless centreline velocity is $U_0 = M$, the centreline Mach number of the flow. In a thin region of width δ near the acoustically lined duct wall, the steady base flow velocity and density vary, giving r-dependent profiles, $U(r)$ and $\rho(r)$. We take the flow to be non-slipping, non-swirling and everywhere parallel, and as such the base pressure is constant across the boundary layer, $p \equiv p_0$. The non-dimensional governing equations are, for completeness,

$$\frac{\partial \rho}{\partial t} + \nabla \cdot (\rho \boldsymbol{u}) = 0, \quad \rho \frac{\mathrm{D}\boldsymbol{u}}{\mathrm{D}t} = -\nabla p, \quad \frac{\mathrm{D}p}{\mathrm{D}t} = \frac{\gamma p}{\rho} \frac{\mathrm{D}\rho}{\mathrm{D}t}. \qquad (2.2a\text{-}c)$$

Small, unsteady perturbations to the base flow are considered, of the form

$$q = \tilde{q}(r) \exp\{\mathrm{i}\omega t - \mathrm{i}kx - \mathrm{i}m\theta\}. \qquad (2.3)$$

The common exponential factor is omitted henceforth. The velocity and density gradients in the base flow boundary layer alter the effect of the acoustic lining on the acoustics. At the lining, the acoustic pressure drives a wall-normal velocity, $\tilde{p} = Z_b\tilde{v}$, for the given impedance of the lining, Z_b. Governing equations for the acoustic pressure $\tilde{p}$ and radial velocity $\tilde{v}$ may be derived from (2.2):

$$\left(\frac{\tilde{p}'}{Q}\right)' + \frac{\bar{\alpha}^2}{Q}\tilde{p} = 0, \quad \left[\left(\frac{r\tilde{v}}{\omega - Uk}\right)' \frac{Q}{\bar{\alpha}^2}\right]' + Q\left(\frac{r\tilde{v}}{\omega - Uk}\right) = 0, \qquad (2.4a,b)$$

where a prime denotes differentiation with respect to r, and

$$Q(r) = \frac{\rho(\omega - Uk)^2}{r} \quad \text{and} \quad \bar{\alpha}(r)^2 = \rho(\omega - Uk)^2 - k^2 - \frac{m^2}{r^2}. \qquad (2.5a,b)$$

It is worth noting that the Pridmore-Brown equation (2.4a) (Pridmore-Brown 1958) and the corresponding equation for the radial velocity (2.4b) are both second order, in $\tilde{p}$ and $\tilde{v}$ respectively, with the radial momentum equation stating $\tilde{v} \sim \tilde{p}'$. The similarity between the two equations (2.4a,b) may be highlighted by defining $\phi = r\tilde{v}/(\omega - Uk)$ and rearranging to give

$$\frac{Q}{\bar{\alpha}^2}\left(\frac{\tilde{p}'}{Q}\right)' + \tilde{p} = 0, \quad \frac{1}{Q}\left(\frac{Q}{\bar{\alpha}^2}\phi'\right)' + \phi = 0. \qquad (2.6a,b)$$

Inherent in the linearisation of the Euler equation, and thus in (2.4a,b), is the so-called critical layer singularity, $\omega - U(r_c)k = 0$, where r_c is the radial location of the critical layer. This occurs when a wave is perfectly convected, and leads to a continuous hydrodynamic spectrum. We neglect the critical layer in this work by assuming that r_c does not fall within our physical domain.

2.1. *The uniform solution*

It is well known (see e.g. Vilenksi & Rienstra 2007; Brambley & Peake 2008) that the acoustic pressure and radial velocity in a duct with inviscid uniform flow can be expressed in terms of Bessel functions as $\tilde{p}_u(r) = EJ_m(\alpha r)$ and $\tilde{v}_u(r) = i\alpha EJ'_m(\alpha r)/(\omega - Mk)$, where $\alpha^2 = (\omega - Mk)^2 - k^2$ and E is a constant amplitude. Modes for such a flow are found by applying a boundary condition at the lined wall, $\tilde{p}_u(1) = Z_{eff}\tilde{v}_u(1)$. The effective impedance Z_{eff} differs from the true lining impedance Z_b due to refraction through the sheared boundary layer, which is neglected in the uniform flow model. For example, for the Myers boundary condition,

$$Z_{eff} = \frac{\omega}{\omega - Mk}Z_b, \qquad (2.7)$$

where the Doppler factor accounts for refraction across a vortex sheet by enforcing continuity of normal displacement. We would like to choose a Z_{eff} such that the easily calculable uniform flow acoustic modes match the modes in the real flow with a sheared boundary layer. Thus, Z_{eff} includes information about both the lining impedance Z_b, and how acoustic modes evolve in shear. This means that solving the uniform flow problem with a lining impedance of Z_{eff} is equivalent to solving the true sheared flow problem with the actual lining impedance Z_b. We are interested in the relationship between Z_b and Z_{eff}.

If we knew both ω and k, then we could find Z_{eff} explicitly:

$$Z_{eff} = (\omega - Mk)\frac{J_m(\alpha)}{i\alpha J'_m(\alpha)}. \tag{2.8}$$

We do not know both k and ω, *a priori*, however, and therefore we would like to solve (2.8) for the modes $k(\omega)$; a relationship between Z_{eff} and the known Z_b is then needed. For example, the Ingard–Myers boundary condition modelling an infinitely thin shear layer (Eversman & Beckemeyer 1972) is given in (2.7), while the first-order asymptotic correction to the Ingard–Myers boundary condition in the limit of a thin shear layer (Brambley 2011*b*) is given by

$$Z_{eff} = \frac{\omega}{\omega - Mk}\frac{Z_b - \dfrac{i(\omega - Mk)^2}{\omega}\delta I_0}{1 + i\omega Z_b\dfrac{k^2 + m^2}{(\omega - Mk)^2}\delta I_1}, \tag{2.9}$$

where I_0 and I_1 are integrals across the thin boundary layer,

$$\delta I_0 = \int_0^1\left(1 - \frac{(\omega - U(r)k)^2\rho(r)}{(\omega - Mk)^2}\right)\mathrm{d}r, \quad \delta I_1 = \int_0^1\left(1 - \frac{(\omega - Mk)^2}{(\omega - U(r)k)^2\rho(r)}\right)\mathrm{d}r. \tag{2.10a,b}$$

2.2. *An impedance governing equation*

Most work concerning acoustic propagation in inviscid fluids begins with equations (2.2) and reduces them to a form of the Pridmore-Brown equation (Pridmore-Brown 1958), e.g. equation (2.4*a*). Less common is the corresponding governing equation for the radial acoustic velocity $\tilde{v}$, equation (2.4*b*). Here, we also work directly with the impedance and derive a new governing equation. We extend the relationship $\tilde{p} = Z_b\tilde{v}$ at the boundary $r = 1$ to one valid for all r, i.e. $Z(r) = \tilde{p}(r)/\tilde{v}(r)$. The same is done for the uniform flow equivalent, i.e. $Z_u(r) = \tilde{p}_u(r)/\tilde{v}_u(r)$. Hence, $Z_b \equiv Z(1)$ and $Z_{eff} \equiv Z_u(1)$.

From (2.2) and (2.4*a,b*) the following relations may be derived:

$$\frac{\bar{\alpha}^2}{Q}\tilde{p} = i\left(\frac{r\tilde{v}}{\omega - Uk}\right)' \quad \text{and} \quad \tilde{p}' = -iQ\left(\frac{r\tilde{v}}{\omega - Uk}\right). \tag{2.11a,b}$$

Guided by the form of (2.11), we write

$$\frac{1}{r}(\omega - Uk)Z = \frac{\tilde{p}}{\dfrac{r\tilde{v}}{(\omega - Uk)}}. \tag{2.12}$$

Taking the derivative with respect to r and using (2.11) to eliminate $\tilde{p}$ and $\tilde{v}$, we find a nonlinear Ricatti equation for Z,

$$\left[\frac{1}{r}(\omega - Uk)Z\right]' = -iQ + \frac{i\bar{\alpha}^2}{Q}\left[\frac{1}{r}(\omega - Uk)Z\right]^2. \tag{2.13}$$

Note that (2.13) is a rephrasing of the acoustic equations (2.4*a,b*), and thus $Z(r)$ represents the lumped impedance of both the boundary and the fluid in $[r, 1]$. Since

(2.13) is a first-order equation and at the lining the boundary condition gives $Z(1) = Z_b$, in the uniform flow region the requirement that $Z(r) = Z_u(r)$ allows us to find Z_{eff}.

The equation (2.13) is exact, and so its numerical solution should correspond with the direct solution of the Pridmore-Brown equation. However, its nonlinearity makes it a less attractive candidate for such computations. Instead we solve (2.13) using two different approximate methods. In §4, two single-step Runge–Kutta solutions are found, one explicit and one implicit, which exploit the inherently small step size δ. In appendix B, an alternative asymptotic analysis (to that in §3) is performed by expanding (2.13) in terms of the small width of the boundary layer, δ. The two methods vary in essence by where we make our approximations: the first approximately solves an exact equation; the second exactly solves an approximate equation.

3. Deriving the asymptotic solution

In this section the asymptotic boundary condition for the effective impedance is found to second order in δ by solving (2.4*a,b*) inside the boundary layer and matching to the uniform solutions outside the boundary layer.

Outside the boundary layer, the uniform base flow pressure solution may be written $\tilde{p}_u(r) = EJ_m(\alpha r)$ as described above. Expanding this about the lined wall at $r = 1$ using the boundary layer scaling $r = 1 - \delta y$ as in Brambley (2011*b*), the outer solution for the pressure becomes

$$\tilde{p}_u(1 - \delta y) = EJ_m(\alpha) - \delta y E\alpha J'_m(\alpha) - \tfrac{1}{2}\delta^2 y^2 E[\alpha J'_m(\alpha) + (\alpha^2 - m^2)J_m(\alpha)] + O(\delta^3). \quad (3.1)$$

Using the notation $p_\infty \equiv \tilde{p}_u(1)$, the pressure at the wall $r = 1$ and $v_\infty \equiv \tilde{v}_u(1)$, equation (3.1) and the equivalent radial velocity expansion may be written as

$$\tilde{p}_u(1 - \delta y) = p_\infty + \delta y i(\omega - Mk)v_\infty$$
$$+ \tfrac{1}{2}\delta^2 y^2[(k^2 + m^2 - (\omega - Mk)^2)p_\infty + i(\omega - Mk)v_\infty] + O(\delta^3), \quad (3.2a)$$

$$\tilde{v}_u(1 - \delta y) = v_\infty - \delta y \left(\frac{(\omega - Mk)^2 - k^2 - m^2}{i(\omega - Mk)}p_\infty - v_\infty \right)$$
$$+ \frac{1}{2}\delta^2 y^2 \left[\frac{3m^2 + k^2 - (\omega - Mk)^2}{i(\omega - Mk)}p_\infty + (2 + k^2 + m^2 - (\omega - Mk)^2)v_\infty \right]$$
$$+ O(\delta^3). \quad (3.2b)$$

Our inner solutions will be matched to (3.2) in the limit $y \to \infty$.

In terms of the boundary layer variable y, equations (2.4*a,b*) become

$$\left(\frac{\tilde{p}_y}{\rho(\omega - Uk)^2} \right)_y = \delta \left(\frac{y\tilde{p}_y}{\rho(\omega - Uk)^2} \right)_y - \delta^2 \left(1 - \frac{k^2 + m^2}{\rho(\omega - Uk)^2} \right)\tilde{p} + O(\delta^3) \quad (3.3)$$

for the pressure, and

$$
\left[\left(\frac{\tilde{v}}{\omega - Uk} \right)_y \frac{\rho(\omega - Uk)^2}{\rho(\omega - Uk)^2 - k^2 - m^2} \right]_y = \delta \left(\frac{\tilde{v}}{\omega - Uk} \frac{\rho(\omega - Uk)^2}{\rho(\omega - Uk)^2 - k^2 - m^2} \right)_y
$$

$$
- \delta \left[\left(\frac{\tilde{v}}{\omega - Uk} \right)_y \frac{2m^2 y \rho(\omega - Uk)^2}{[\rho(\omega - Uk)^2 - k^2 - m^2]^2} \right]_y - \delta^2 \left(\frac{\tilde{v}}{\omega - Uk} \rho(\omega - Uk)^2 \right)
$$

$$
+ \delta^2 \left(\frac{\tilde{v}}{\omega - Uk} \frac{y \rho(\omega - Uk)^2}{[\rho(\omega - Uk)^2 - k^2 - m^2]^2} (\rho(\omega - Uk)^2 + m^2 - k^2) \right)_y
$$

$$
- \delta^2 \left[\left(\frac{\tilde{v}}{\omega - Uk} \right)_y \frac{4m^2 y^2 \rho(\omega - Uk)^2}{[\rho(\omega - Uk)^2 - k^2 - m^2]^3} (\rho(\omega - Uk)^2 - k^2) \right]_y + O(\delta^3) \quad (3.4)
$$

for the radial velocity. Here ρ and U are now the corresponding base density and axial velocity as functions of y. A subscript denotes differentiation.

Solving (3.3) and (3.4) to second order produces the inner solutions (see appendix A for details). When evaluated at the wall, the second-order correction to the $\tilde{v}$ expansion is singular if $(\omega - Mk)^2 = k^2 + m^2$. Solutions of the Pridmore-Brown equation exist at this point. Thus, the singularity is a consequence of the asymptotic expansion and is spurious. Close to the new singular point, one could simply revert to using the first-order expansion as derived by Brambley (2011b), which is unaffected by the unphysical singularity.

Matching with the outer solutions (3.2) and evaluating at the boundary $y = 0$ gives, after some algebra,

$$
\begin{aligned}
\tilde{p}(0) = {} & \tilde{p}_u(0) + i(\omega - Mk)\tilde{v}_u(0)\delta I_0 + i(\omega - Mk)\tilde{v}_u(0)\delta^2 I_2 \\
& + (k^2 + m^2)\tilde{p}_u(0)(\delta I_0 \delta I_1 - \delta^2 I_3) - (\omega - Mk)^2 \tilde{p}_u(0)\delta^2 I_7 + O(\delta^3), \quad (3.5a)
\end{aligned}
$$

$$
\begin{aligned}
\tilde{v}(0) = {} & \frac{\omega}{\omega - Mk} \left\{ \tilde{v}_u(0) - i\tilde{p}_u(0) \frac{k^2 + m^2}{\omega - Mk} \delta I_1 + (\omega - Mk)^2 \tilde{v}_u(0)\delta^2 I_2 \right. \\
& + (k^2 + m^2)\tilde{v}_u(0)\delta^2 I_3 + i\tilde{p}_u(0) \frac{k^2 + m^2}{\omega - Mk} \frac{k^2 - m^2 - (\omega - Mk)^2}{k^2 + m^2 - (\omega - Mk)^2} \delta^2 I_3 \\
& + (k^2 + m^2)\tilde{v}_u(0)(\delta I_0 \delta I_1 - \delta^2 I_2 - \delta^2 I_5) \\
& \left. + \frac{2im^2 \tilde{p}_u(0)}{\omega - Mk} \left(\frac{k^2 + m^2}{k^2 + m^2 - (\omega - Mk)^2} \delta^2 I_6 - \delta^2 I_4 \right) \right\} + O(\delta^3), \quad (3.5b)
\end{aligned}
$$

where the integrals I_j are

$$
\begin{aligned}
& I_0 = \int_0^\infty \chi_0(y) \, dy, \quad I_1 = \int_0^\infty \chi_1(y) \, dy, \quad I_2 = \int_0^\infty y \chi_0(y) \, dy, \\
& I_3 = \int_0^\infty y \chi_1(y) \, dy, \quad I_4 = \int_0^\infty y \chi_2(y) \, dy, \quad I_5 = \int_0^\infty \chi_1(y) \int_0^y \chi_0(y') \, dy' \, dy, \\
& I_6 = \int_0^\infty y \chi_1(y) \chi_2(y) \, dy, \quad I_7 = \int_0^\infty \chi_0(y) \int_0^y \left(1 - \frac{k^2 + m^2}{\rho(y')(\omega - U(y')k)^2} \right) dy' \, dy,
\end{aligned}
$$
$$(3.6)$$

with

$$\chi_0(y) = \left[1 - \frac{\rho(\omega - Uk)^2}{(\omega - Mk)^2}\right], \quad \chi_1(y) = \left[1 - \frac{(\omega - Mk)^2}{\rho(\omega - Uk)^2}\right],$$

$$\chi_2(y) = \left[1 - \frac{(\omega - Mk)^2 - k^2 - m^2}{\rho(\omega - Uk)^2 - k^2 - m^2}\right].$$

(3.7)

The impedance of the boundary is the ratio of the acoustic pressure to the normal velocity that it drives, so we write $Z_b = \tilde{p}(0)/\tilde{v}(0)$ using (3.5). We identify the effective impedance with the same ratio for the uniform flow variables: $Z_{eff} = p_\infty/v_\infty$. Using these two relationships, we may rearrange the ratio of (3.5a) and (3.5b) to find an expression for the effective impedance of an acoustic liner with an inviscid sheared boundary layer:

$$Z_{eff} = \frac{\omega}{\Omega_u} \frac{Z_b - \dfrac{i\Omega_u^2}{\omega}(\delta I_0 + \delta^2 I_2) - Z_b \mu^2 \delta^2 I_2 + \sigma_+ Z_b(\delta I_0 \delta I_1 + \delta^2 I_3 - \delta^2 I_5)}{1 + i\sigma_+ \dfrac{\omega Z_b}{\Omega_u^2}\delta I_1 + \Upsilon_1 \delta^2 I_3 + \Upsilon_2\left(\delta^2 I_4 - \dfrac{\sigma_+}{\mu^2}\delta^2 I_6\right) + \sigma_+ \delta I_0 \delta I_1 - \Omega_u^2 \delta^2 I_7} + O(\delta^3),$$

(3.8)

where $\sigma_+ = k^2 + m^2$, $\Omega_u = \omega - Mk$ and $\mu^2 = \sigma_+ - \Omega_u^2$, and where

$$\Upsilon_1 = \frac{i\sigma_+ \omega Z_b}{\Omega_u^2}\left(\frac{2m^2}{\mu^2} - 1\right) - \sigma_+, \quad \Upsilon_2 = 2im^2 \frac{\omega Z_b}{\Omega_u^2}.$$

(3.9a,b)

Equation (3.8) readily reduces to the modified boundary condition as derived by Brambley (2011b) at $O(\delta)$, equation (2.9), and to the classical Myers condition (2.7) in the limit $\delta \to 0$. Figure 1 shows that the condition is correct to the stated asymptotic order.

Equation (3.8) may be applied in the physical r domain by transforming the integrals I_j as follows:

$$\delta I_0 = \int_0^1 \chi_0(r)\,dr, \quad \delta I_1 = \int_0^1 \chi_1(r)\,dr, \quad \delta^2 I_2 = \int_0^1 (1-r)\chi_0(r)\,dr,$$

$$\delta^2 I_3 = \int_0^1 (1-r)\chi_1(r)\,dr, \quad \delta^2 I_4 = \int_0^1 (1-r)\chi_2(r)\,dr,$$

$$\delta^2 I_5 = \int_0^1 \chi_1(r)\int_r^1 \chi_0(r')\,dr'\,dr, \quad \delta^2 I_6 = \int_0^1 (1-r)\chi_1(r)\chi_2(r)\,dr,$$

$$\delta^2 I_7 = \int_0^1 \chi_0(r)\int_r^1 \left(1 - \frac{\sigma_+}{\rho(r')\Omega(r')^2}\right)\,dr'\,dr.$$

(3.10)

An example of the accuracy of this boundary condition is given in §5, and an explicit form for a linear boundary layer profile is given in §6.1.

4. The Runge–Kutta solutions

Here we derive an expression for Z_{eff} by approximately solving (2.13) using a single step of a fourth-order explicit Runge–Kutta method (see Hairer, Nørsett & Wanner 1993), and a second-order, single-step implicit scheme.
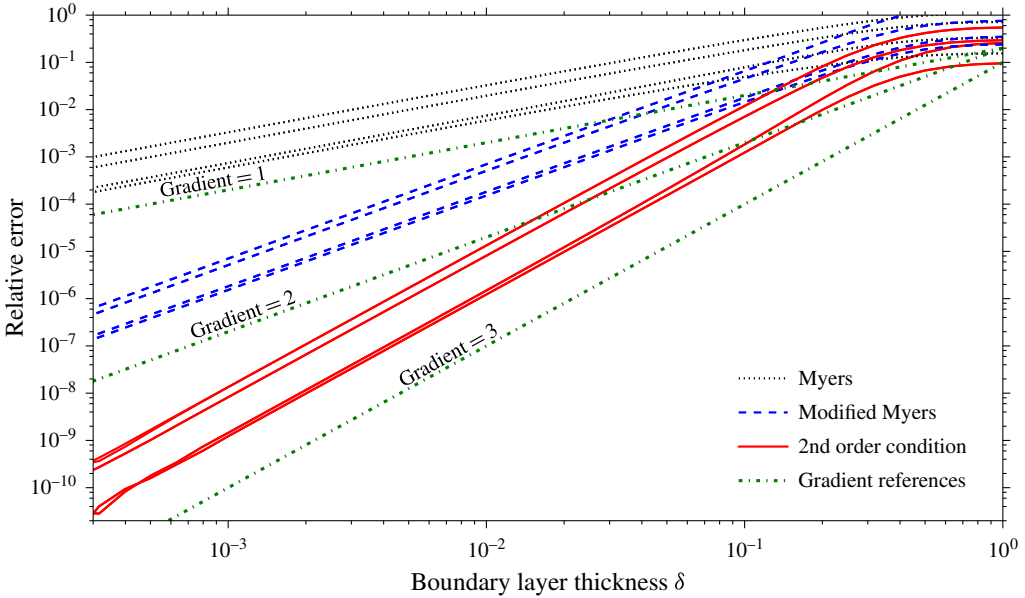
FIGURE 1. (Colour online) The relative errors of the leading (black dotted), first (blue dashed) and second (red solid) orders of the new boundary condition (3.8) when compared with numerical solutions of the Pridmore-Brown equation. The green dash-dotted lines have gradients of 1, 2 and 3 beginning from the top and moving down. Parameters used are $k = \pm 1 \pm i$, $\pm i$ and $\omega = 1$, $m = 0$, $M = 0.5$ with the tanh boundary layer profile of (5.1). Relative error is defined by $|Z^*/Z_{eff} - 1|$, where Z^* is the approximation from the specified model, and Z_{eff} is the exact result from (2.8).

Equation (2.13) may be transformed as follows. Dividing (2.13) through by $(\omega - Mk)^2$ produces

$$\frac{1}{\omega - Mk}L' = -i\tilde{Q} + \frac{i\bar{\alpha}^2}{\tilde{Q}(\omega - Mk)^2}L^2, \tag{4.1}$$

where $\tilde{Q} = Q/(\omega - Mk)^2$, an $O(1)$ quantity for all ω, k, and

$$L = \frac{(\omega - Uk)}{r(\omega - Mk)}Z. \tag{4.2}$$

The quantity L may be split into a uniform flow value, $L_u = Z_u/r$, and a perturbation due to the presence of the boundary layer, $\tilde{L}$, such that

$$L = L_u + \tilde{L}. \tag{4.3}$$

Equation (4.1) has the associated data $L_u(1) = Z_{eff}$, and $L = L_u$ outside the boundary layer. For a uniform flow of Mach number M and constant density $\rho \equiv 1$, (4.1) reduces to

$$\frac{1}{(\omega - Mk)}L'_u = -\frac{i}{r} + ir\left(1 - \frac{k^2 + \dfrac{m^2}{r^2}}{(\omega - Mk)^2}\right)L_u^2. \tag{4.4}$$

Equation (4.4) may then be used in (4.1) along with the decomposition (4.3) to form a governing equation for $\tilde{L}(r)$:

$$
\frac{1}{(\omega - Mk)}\tilde{L}' = \frac{i}{r}\left[1 - \frac{\rho(\omega - Uk)^2}{(\omega - Mk)^2}\right] + ir\frac{k^2 + \dfrac{m^2}{r^2}}{(\omega - Mk)^2}\left[1 - \frac{(\omega - Mk)^2}{\rho(\omega - Uk)^2}\right]L_u^2
$$

$$
+ ir\left[1 - \frac{k^2 + \dfrac{m^2}{r^2}}{\rho(\omega - Uk)^2}\right](2L_u\tilde{L} + \tilde{L}^2). \tag{4.5}
$$

The asymptotics of (4.5) may be found in appendix B, where it is shown that the modified Myers (Brambley 2011*b*) condition may be cleanly reproduced from (4.5) but the second-order extension runs into difficulties concerning non-uniqueness. Here, we proceed with approximate solutions to (4.5).

4.1. *The explicit scheme*

In order to ensure the correct $\delta \to 0$ behaviour, we use the decomposition (4.3) and solve (4.5) for $\tilde{L}(r)$, with the necessary condition that $\tilde{L} = 0$ in uniform flow (for $r < 1 - \delta$). While this is technically only valid for profiles with $U \equiv M$ for $r < 1 - \delta$, for a 99 % U_0 boundary layer thickness the approximation $\tilde{L} = 0$ for $r < 1 - \delta$ is a reasonable one. We choose to step from the top of the boundary layer at $r = 1 - \delta$, with the initial condition $\tilde{L}(1 - \delta) = 0$, to the lining at $r = 1$, where the boundary condition $\tilde{L}(1) = \omega Z_b/(\omega - Mk) - Z_{eff}$ gives Z_{eff} as a function of Z_b. Using the analytic uniform solution defined in § 2.1, we can treat as known the intermediate values of $L_u(r)$ that arise.

To perform the step, we define the fourth-order explicit Runge–Kutta difference equation $\tilde{L}_1 = \tilde{L}_0 + \delta/6(k_1 + 2k_2 + 2k_3 + k_4)$, where $\tilde{L}_0 = \tilde{L}(1 - \delta) = 0$. Defining

$$
A = \frac{i(\omega - Mk)}{r}\chi_0, \quad B = ir\frac{k^2 + m^2/r^2}{\omega - Mk}\chi_1, \quad C = ir(\omega - Mk)\left[1 - \frac{k^2 + m^2/r^2}{\rho(\omega - Uk)^2}\right], \tag{4.6a-c}
$$

with χ_j defined as in (3.7), the k_j terms become

$$
k_1 = A(1 - \delta) + B(1 - \delta)L_u(1 - \delta)^2, \tag{4.7a}
$$

$$
k_2 = A(1 - \delta/2) + B(1 - \delta/2)L_u(1 - \delta/2)^2 + C(1 - \delta/2)\left(2L_u(1 - \delta/2)\frac{\delta}{2}k_1 + \frac{\delta^2}{4}k_1^2\right), \tag{4.7b}
$$

$$
k_3 = A(1 - \delta/2) + B(1 - \delta/2)L_u(1 - \delta/2)^2 + C(1 - \delta/2)\left(2L_u(1 - \delta/2)\frac{\delta}{2}k_2 + \frac{\delta^2}{4}k_2^2\right), \tag{4.7c}
$$

$$
k_4 = A(1) + B(1)Z_{eff}^2 + C(1)(2Z_{eff}\delta k_3 + \delta^2 k_3^2). \tag{4.7d}
$$

The decomposition (4.3) may then be used to apply the boundary condition at $r = 1$, giving

$$
Z_{eff} = \frac{\omega}{\omega - Mk}Z_b - \frac{\delta}{6}(k_1 + 2k_2 + 2k_3 + k_4). \tag{4.8}
$$

If we extract the Z_{eff} from k_4, defining $k_4 = \tilde{k}_4 + [B(1)Z_{eff} + 2C(1)\delta k_3]Z_{eff}$, where $\tilde{k}_4 = A(1) + \delta^2 C(1)k_3^2$, we can rearrange (4.8) to find

$$Z_{eff} = \frac{\omega}{\omega - Mk} \frac{Z_b - \dfrac{\delta}{6}(1 - Mk/\omega)(k_1 + 2k_2 + 2k_3 + \tilde{k}_4)}{1 + \dfrac{\delta}{6}(B(1)Z_{eff} + 2\delta C(1)k_3)}, \tag{4.9}$$

which then gives Z_{eff} as a function of Z_b. The classical Myers condition is recovered in the limit $\delta \to 0$, as we would hope (Eversman & Beckemeyer 1972; Tester 1973a). The form of (4.9) bears a striking resemblance to that of the modified Myers condition.

4.2. *A single-step implicit scheme*

Here we define a trapezoidal second-order, single-step implicit Runge–Kutta scheme and use it for a single step to approximate Z_{eff}. For this scheme, the fundamental difference equation for the differential equation $y' = f(x, y)$ is

$$y_{n+1} = y_n + \frac{h}{2}(f(x_n, y_n) + f(x_{n+1}, y_{n+1})). \tag{4.10}$$

The method is implicit due to the appearance of y_{n+1} on both sides of (4.10).

We use the scheme to first step back from the boundary, which has a known impedance Z_b, through the sheared boundary layer profile to the edge of the boundary layer at $r = 1 - \delta$; and then to step forward from $r = 1 - \delta$ to $r = 1$ assuming a uniform flow. The details of these steps are found in appendix D.

The method results in the effective impedance

$$Z_{eff} = X_1 + \tfrac{1}{2}\delta(\tilde{k}_1 + \tilde{k}_2), \tag{4.11}$$

where

$$X_1 = X_0 - \frac{1}{2}\delta(k_1 + k_2) \quad \text{and} \quad X_0 = \frac{\omega}{\omega - Mk}Z_b, \tag{4.12a,b}$$

with

$$k_1 = A_1(1) + B_1(1)X_0^2, \tag{4.13}$$

$$k_2 = \left(\frac{2}{\delta^2 B_1(1-\delta)} + 2\frac{X_0}{\delta} - k_1\right)$$
$$\times \left(1 - \left\{1 - \frac{4A_1(1-\delta)/B_1(1-\delta) + (2X_0 - \delta k_1)^2}{\left(\dfrac{2}{\delta B_1(1-\delta)} + 2X_0 - \delta k_1\right)^2}\right\}^{1/2}\right), \tag{4.14}$$

for

$$A_1(r) = -\frac{i}{r}\frac{\rho(\omega - Uk)^2}{\omega - Mk}, \quad B_1(r) = ir(\omega - Mk)\left(1 - \frac{k^2 + m^2/r^2}{\rho(\omega - Uk)^2}\right), \tag{4.15a,b}$$

and with

$$\tilde{k}_1 = A_2(1-\delta) + B_2(1-\delta)X_1^2, \qquad (4.16)$$

$$\tilde{k}_2 = \left(\frac{2}{\delta^2 B_2(1)} - 2\frac{X_1}{\delta} - \tilde{k}_1\right)\left(1 - \left\{1 - \frac{4A_2(1)/B_2(1) + (2X_1 + \delta\tilde{k}_1)^2}{\left(\frac{2}{\delta B_2(1)} - 2X_1 - \delta\tilde{k}_1\right)^2}\right\}^{1/2}\right), \quad (4.17)$$

for

$$A_2(r) = -\frac{\mathrm{i}}{r}(\omega - Mk), \quad B_2(r) = \mathrm{i}r(\omega - Mk)\left(1 - \frac{k^2 + m^2/r^2}{(\omega - Mk)^2}\right). \quad (4.18a,b)$$

The two steps used here (back then forward) allow the resulting condition to be a direct map from Z_b to Z_{eff} (like the asymptotic boundary condition (3.8)), without intermediate values of Z_u having to be used (as in the explicit Runge–Kutta scheme (4.9)).

5. Accuracy of models of Z_{eff}

To measure the accuracy of the boundary conditions derived above, numerical solutions of the full Pridmore-Brown equation were found. This was achieved using a sixth-order finite difference discretisation on a computational grid spaced uniformly in ξ, where $r = \tanh(A\xi)/\tanh(A)$, and A is a stretching parameter, in order to cluster points near $r = 1$ to resolve the boundary layer. Regularity conditions were imposed at $r = 0$, and the wall boundary condition was $\tilde{p}(1) = 1$, with $\tilde{v}$ free. Roots of the dispersion relation $Z_b = \tilde{p}/\tilde{v}$ were found via Newton–Raphson iteration over k. The tanh velocity profile (Rienstra & Vilenski 2008)

$$U(r) = M\tanh\left(\frac{1-r}{\delta}\right) + M(1 - \tanh(1/\delta))\left(\frac{1 + \tanh(1/\delta)}{\delta}r + (1+r)\right)(1-r), \tag{5.1}$$

was used to generate the following results, with a constant density $\rho(r) \equiv 1$. This base flow has a displacement thickness

$$\delta^* = \frac{1}{6\delta}(\tanh^2(1/\delta) - 1) + \frac{1}{3}(1 + 2\tanh(1/\delta)) - \delta\ln(\cosh(1/\delta)), \tag{5.2}$$

which for $\delta \in (10^{-7}, 10^{-1})$ gives $\delta^*/\delta = 0.69$ to two decimal places.

A good initial test of the boundary conditions, and one which seems to be missing from the literature concerning such impedance boundary conditions, is to directly check how well the effective impedance is approximated. By solving the Pridmore-Brown equation throughout the complex k-plane for a given ω and m, a boundary impedance Z_b is generated at each k. This solution has a unique uniform flow equivalent and the value of $Z_u(1)$ of this uniform flow mode, from (2.8), is the Z_{eff} against which we test the models.

Figure 2 shows the absolute errors in the complex k-plane of the predicted Z_{eff} for each boundary condition. For the thin boundary layer thickness $\delta = 2 \times 10^{-3}$, the asymptotic conditions perform well. As one would expect, the $O(\delta^2)$ asymptotic
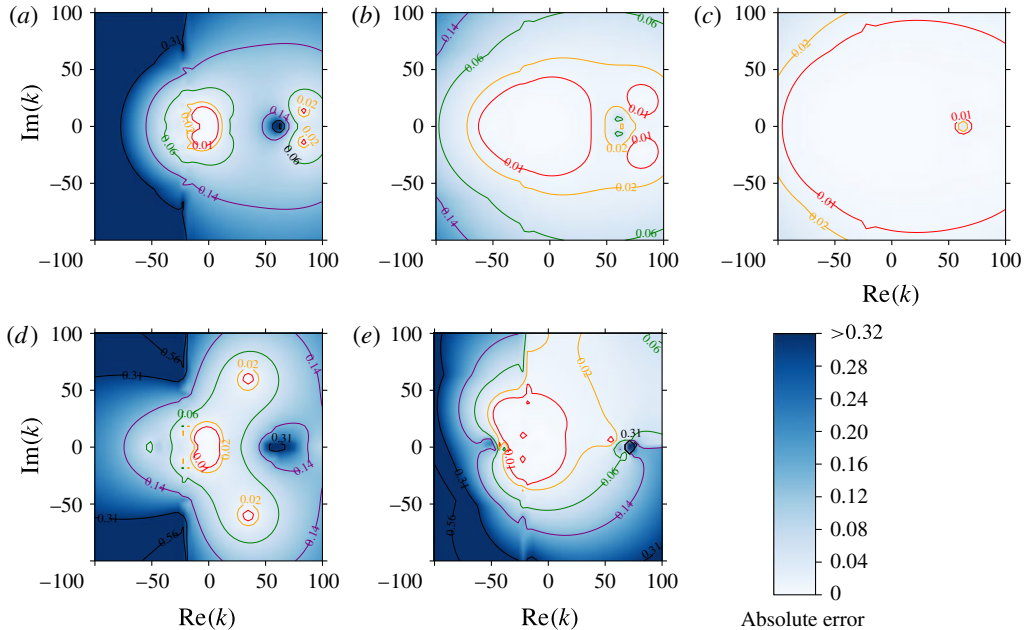
FIGURE 2. (Colour online) Absolute errors in the complex k-plane of the predicted Z_{eff} for each boundary condition. The colour scheme is normalised such that the darkest blue is an error greater than or equal to 1.5 times the mean Myers error. The red contour surrounds errors lower than the lowest quartile of the five plotted data sets combined. Shown are (a) the Myers condition (2.7), (b) the modified Myers condition (2.9), (c) the second-order $O(\delta^2)$ asymptotic condition (3.8), (d) the single-step implicit Runge–Kutta condition (4.11) and (e) the explicit Runge–Kutta condition (4.9). The error was calculated as $\min\{|Z_1 - Z_2|, |1/Z_1 - 1/Z_2|\}$. Parameters are $\omega = 31$, $m = 24$, $M = 0.5$, $\delta = 2 \times 10^{-3}$, for a tanh velocity profile (5.1) and constant base density $\rho(r) \equiv 1$. The boundary impedance at each point is found from the numerical solution of the Pridmore-Brown equation, (2.4a).

solution, figure 2(c), is more accurate throughout the plotted domain than the modified Myers condition, figure 2(b), which in turn is more accurate than the Myers condition, figure 2(a). For the parameters $\omega = 31$ and $m = 24$ (typical values for rotor-alone noise in an aeroengine bypass duct at take-off (McAlpine *et al.* 2006)), and the restriction to $\mathrm{Im}(k), \mathrm{Re}(k) \in [-100, 100]$, we are well within the region of asymptotic validity, $\omega, m, k \ll 1/\delta$. The single-step explicit Runge–Kutta scheme, figure 2(e), performs well in regions where the scheme is stable, but blows up erratically due to the stiffness of the impedance Ricatti equation (2.13). The single-step implicit scheme, figure 2(d), is reasonably accurate for most of the domain, but has regions where the error is large. Sudden changes inside the boundary layer are not modelled well by the implicit scheme, which utilises data points only at either side of the layer; this suggests that the implicit scheme is not suitable for predicting surface modes, and may explain the loss of accuracy of the implicit scheme in the darker regions of figure 2(d). The Myers condition, figure 2(a), also loses accuracy in these regions due to its vanishingly thin shear layer. The well-posed asymptotic schemes in figure 2(b,c) do not have this problem: the bulk treatment of the shear as integrals across the boundary layer, equation (3.6), allow better modelling of variations inside the boundary layer.
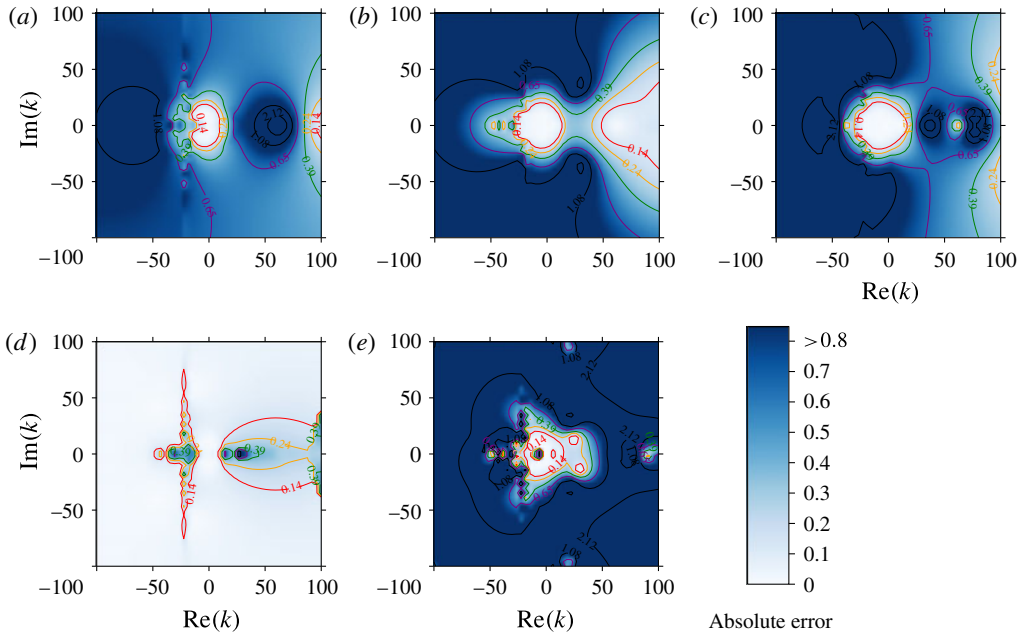
FIGURE 3. (Colour online) As in figure 2, but for a boundary layer thickness $\delta = 3 \times 10^{-2}$. Note also the different error scale compared with figure 2.

In the bypass duct of an aeroengine, the boundary layer may be much thicker than 10^{-3}. Figure 3 shows results for $\delta = 3 \times 10^{-2}$, with all other parameters as in figure 2. For this relatively thick boundary layer, the region of asymptotic validity is $k \ll 33$, so it is no surprise that the breakdown of the asymptotic models (figure 3b,c) occurs within the plotted domain. The Myers condition, figure 3(a), is also only usefully accurate in a small region near the origin. The instability of the explicit method makes it unusable in most circumstances (figure 3e). The A-stable single-step implicit scheme, however, comes into its own for thicker boundary layers. Figure 3(d) shows the implicit scheme to be extremely accurate throughout the k domain. Importantly, the accuracy is not lessened as k increases past $1/\delta$, meaning that the single-step implicit scheme may also be useful when short-wavelength, high-frequency waves interact with a thick boundary layer. There are, however, larger errors near the Doppler-shifted origin, which is a region important for modes close to cut-on. These errors can manifest as erroneous instabilities of the least cut-off upstream modes, discussed in § 7.

6. Simplified forms and limiting cases

Although expressible analytically, the boundary condition in (3.8) contains integrals across the boundary layer that for a general boundary layer profile must be performed numerically. The single-step implicit scheme boundary condition (4.11) is also complicated in its most general form. We now investigate specific situations when fully closed, simplified forms of the conditions may be found.

6.1. *Linear boundary profile*

In the case of a linear boundary layer velocity profile,

$$U(r) = \begin{cases} M(1-r)/\delta, & (1-r) < \delta, \\ M, & (1-r) > \delta, \end{cases} \tag{6.1}$$

with a constant density $\rho \equiv 1$, the integrals I_j in (3.8) may be performed analytically and a closed-form expression for the $O(\delta^2)$ asymptotic solution can be written:

$$Z_{eff} = \frac{\omega}{\omega - Mk} \frac{Z_b + \delta\dfrac{iMk}{3\omega}(3\omega - 2Mk) + \delta^2 \dfrac{Mk}{12\omega}(8Z_b(k^2 + m^2) - (\omega Z_b - i)(4\omega - 3kM))}{1 + i\delta MkZ_b\dfrac{(k^2 + m^2)}{(\omega - Mk)^2} + \delta^2 \Upsilon_3}, \tag{6.2}$$

where

$$\begin{aligned} \Upsilon_3 &= \frac{Mk}{12(\omega - Mk)^2} \left(Mk^3(4 - 3M^2) + 2k^2(5M^2 - 4)\omega \right. \\ &\quad + Mk(4m^2 - 11\omega^2) - 8m^2\omega + 4\omega^3) \\ &\quad - 6iMk\omega Z(m^2 - k^2)(2\omega - 3Mk) + \frac{i\omega Z_b}{k^2 M^2}(m^2 - k^2)\ln\left(\frac{\omega}{\omega - Mk}\right). \end{aligned} \tag{6.3}$$

Equation (6.2), with (6.3), may be applied directly as a boundary condition assuming a uniform base flow.

The single-step implicit scheme (4.11) simplifies greatly for the specific linear shear profile (6.1). Using the sign convention for the roots as discussed in appendix D, the boundary condition reduces to

$$Z_{eff} = \frac{i\Omega_u}{\delta\mu^2} - \frac{i\Omega_u}{\delta\mu^2}\left\{1 + \frac{\delta Z_b \mu^2}{\Omega_u^2}(2i\omega + \delta(\omega^2 - k^2 - m^2)Z_b) - \delta^2 Mk\mu^2\frac{(2\omega - Mk)}{\Omega_u^2}\right\}^{1/2}, \tag{6.4}$$

where, as before, $\Omega_u = \omega - Mk$ and $\mu^2 = k^2 + m^2 - \Omega_u^2$. Expanding the square root in the small-δ limit recovers the Myers condition at leading order.

Recent work has shown that the shape of the boundary layer profile is not as important for attenuation predictions as parameters such as the displacement and momentum thicknesses (Gabard 2013). Thus, the explicit forms (6.2) and (6.4) could be used more generally if the thickness is altered to match the required boundary layer parameters.

As an example, the displacement thickness for a compressible flow may be defined,

$$\delta^* = \int_0^1 \left(1 - \frac{\rho(r)U(r)}{\rho_0 U_0}\right) dr, \tag{6.5}$$

where a subscript 0 denotes a duct centreline value. Given a displacement thickness of a boundary layer profile that we wish to emulate, we could define a linear profile of the form (6.1) with $\delta \to 2\delta^*$. Momentum thickness and energy thickness might similarly be used.

6.2. *Surface modes*

Surface modes are waves localised near the boundary that decay exponentially into the core of the duct. A surface with a finite impedance (not hard wall) and an infinitesimally thin boundary layer can support up to four surface modes (Rienstra 2003). Working to first order in a finite boundary layer thickness above such a surface allows up to six surface modes to be supported (Brambley 2013). To investigate the effect of the second-order corrections to the surface mode predictions, we utilise the scaling $k/\omega \gg 1$ and the surface mode dispersion relation (Brambley 2013)

$$\mu - \frac{\omega - Mk}{\mathrm{i}Z_{eff}} = 0, \tag{6.6}$$

where Z_{mod} in Brambley (2013) translates to the notation used here as $\mathrm{i}\omega Z_{mod} = \mathrm{i}(\omega - Mk)Z_{eff}$, and $\mu^2 = k^2 + m^2 - (\omega - Mk)^2$, with $\mathrm{Re}(\mu) > 0$. By rearranging (3.8) such that we have $\mathrm{i}(\omega - Mk)Z_{eff} = f(Z_b, Z_{eff})$, and using from (2.8)

$$Z_{eff} = (\omega - Mk)\frac{\mathrm{J}_m(\alpha)}{\mathrm{i}\alpha \mathrm{J}'_m(\alpha)} \quad \text{and} \quad \frac{\mathrm{J}_m(\alpha)}{\alpha \mathrm{J}'_m(\alpha)} \sim \frac{1}{\mu} \tag{6.7a,b}$$

in the function $f(Z_b, Z_{eff})$, the surface mode dispersion relation (6.6) for the $O(\delta^2)$ asymptotic solution may be written as

$$
\begin{aligned}
0 = {} & \mathrm{i}\omega Z_b \left[\mu - \mu^3\delta^2 I_2 + \mu(k^2 + m^2)(\delta I_0 \delta I_1 + \delta^2 I_3 - \delta^2 I_5) \right. \\
& - (k^2 + m^2)\left(\delta I_1 + \left(\frac{2m^2}{\mu^2 - 1} \right)\delta^2 I_3 \right) \\
& \left. - 2m^2\left(\delta^2 I_4 - \frac{1}{\mu^2}(k^2 + m^2)\delta^2 I_6 \right) \right] + \mu(\omega - Mk)^2(\delta I_0 + \delta^2 I_2) \\
& + (k^2 + m^2)(\omega - Mk)^2(\delta^2 I_3 - \delta I_0 \delta I_1) + (\omega - Mk)^4 \delta^2 I_7 - (\omega - Mk)^2.
\end{aligned} \tag{6.8}
$$

To use the dispersion relation (6.8), the I_j integral terms must be evaluated in the regime $k/\omega \gg 1$ (or, in some cases, the wavenumber and frequency dependence extracted from the integrals). For the integrals I_0, I_1, I_2, I_4 and I_7, this may be readily done. For the integrals I_3, I_5 and I_6, however, global contributions are important, and, as such, the k dependence cannot be extracted for a general boundary layer profile. To overcome this problem, the high-k/ω limit of the analytical results for a linear profile are used. This is, of course, detrimental to the resulting surface mode model, but it should give an idea of the number of possible new surface modes predicted by the second-order model. The asymptotic forms of the I_j integrals are shown in appendix C. Using these in (6.8) produces a polynomial in k of order 14 if we take Z_b to be locally reacting (independent of k), meaning that, for a given frequency ω, the $O(\delta^2)$ asymptotic solution predicts the existence of a possible 14 surface modes. Not all of these solutions will correspond to real modes, however, since they must satisfy $\mathrm{Re}(\mu) > 0$ in order to decay away from the boundary. The surface mode asymptotics of the Modified Myers condition by Brambley (2013) predict only six possible surface modes. This suggests that either the modified Myers condition fails to predict all possible surface modes (through the neglect of important physics, say); or the new second-order model predicts spurious modes that are not shared by the Pridmore-Brown equation.
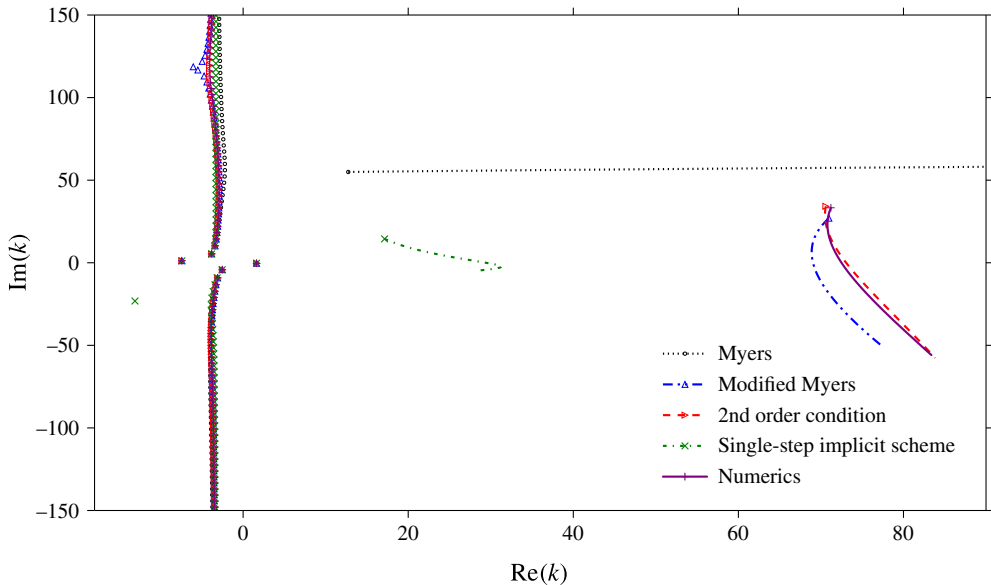
FIGURE 4. (Colour online) Modes in the k-plane of the Myers condition (black circle), modified Myers condition (blue triangle), single-step implicit scheme (4.11) (green cross), $O(\delta^2)$ asymptotic solution (3.8) (red right-pointing triangle) and Pridmore-Brown numerics (purple plus sign). The tanh boundary layer profile (6.1) is used, with a constant base density. Parameters are $\omega = 5$, $m = 0$, $M = 0.5$ and $\delta = 2 \times 10^{-3}$. The boundary impedance for the markers is $Z_b = 3 + 0.52\mathrm{i}$. The lines track the surface mode for each boundary condition as $\mathrm{Im}(\omega)$ is reduced from zero to -10, or sufficiently negative, as $\mathrm{Re}(\omega)$ is held constant, and the boundary impedance changes in line with (7.1).

Repeating the above surface mode analysis for the single-step implicit Runge–Kutta scheme (6.4) produces a sixth-order polynomial in k, meaning a possible six surface modes for a given frequency. This matches the number predicted by the modified Myers condition (Brambley 2013), and suggests that the extra surface modes predicted by the second-order asymptotic condition derived here are in fact spurious. This is investigated further in the next section.

7. Wavenumber spectrum and stability

Modes in the k-plane are found for the Myers, the modified Myers, the single-step implicit scheme (4.11) and the $O(\delta^2)$ asymptotic solution (3.8), and compared with those found via numerical solution of the full Pridmore-Brown equation. The liner model used for all results here (unless specifically stated) is a mass–spring–damper impedance,

$$Z_b(\omega) = R + \mathrm{i}\omega d - \mathrm{i}b/\omega, \tag{7.1}$$

for $R = 3$, $d = 0.15$ and $b = 1.15$. Figure 4 shows the results for a tanh boundary layer profile with a boundary impedance of $Z_b = 3 - 0.52\mathrm{i}$ and parameters $\omega = 5$, $m = 0$ and $\delta = 2 \times 10^{-3}$. In figure 4, the $O(\delta^2)$ asymptotic solution is seen to reproduce the full numerical modes with great accuracy. The single-step implicit condition predicts poorly the surface mode position in the right half-plane, but this is expected: the method cannot fully resolve a wave existing predominantly in the boundary layer;
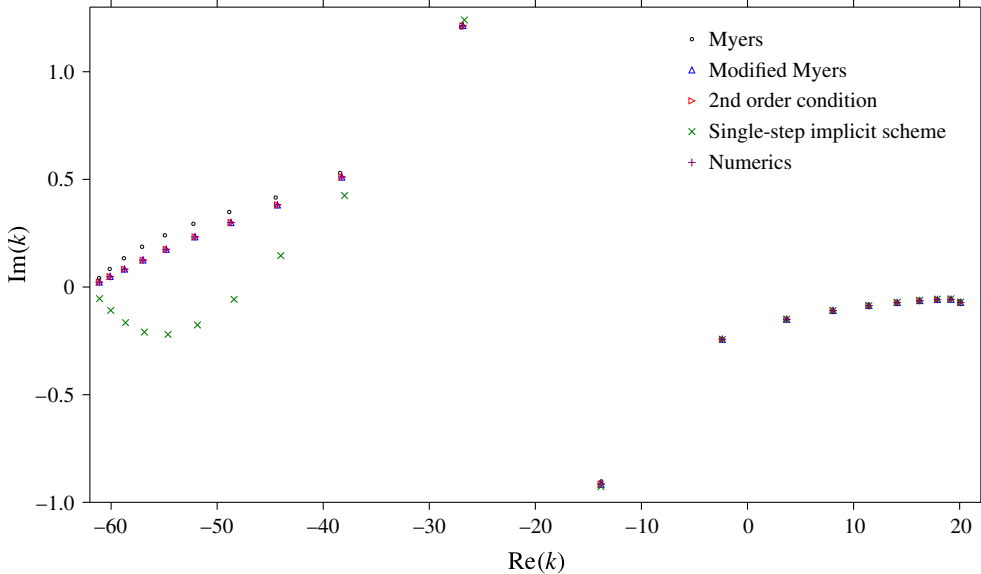
FIGURE 5. (Colour online) Least cut-off modes of the Myers condition (black circle), modified Myers condition (blue triangle), single-step implicit scheme (4.11) (green cross), $O(\delta^2)$ asymptotic solution (3.8) (red right-pointing triangle) and Pridmore-Brown numerics (purple plus sign), for $\omega = 31$, $m = 4$, $M = 0.5$, $\delta = 2 \times 10^{-3}$ and a tanh profile. The boundary impedance is $Z_b = 3 + 4.61\mathrm{i}$.

only information at the top and bottom edges of the boundary layer are used in the numerical scheme. The Myers condition cannot predict the position or behaviour of surface modes (see figure 4), as it neglects boundary layer physics in favour of a vortex sheet.

The lines from the surface modes in the right half-plane of figure 4 are Briggs–Bers (Briggs 1964; Bers 1983) contours, and give us information about the stability of the modes (see the appendix of Brambley (2009) for a full discussion). The modes are tracked as $\mathrm{Im}(\omega)$ is reduced from zero to sufficiently negative. The impedance changes with ω via (7.1). All of the boundary conditions except the Myers condition predict a downstream-propagating convective instability, due to their crossing the real k-axis from the upper to the lower half-planes. This convective instability is also present in the Pridmore-Brown numerics, visible in figure 4.

Figure 5 shows the least cut-off modes in the k-plane for parameters typical of rotor–stator interaction in a turbofan engine. The downstream-propagating modes in the right half of figure 5 are well approximated by all the tested models. Discrepancies can be seen in the upstream-propagating modes of the Myers condition and single-step implicit scheme, however. The Myers condition modes are too cut-off, which could be an explanation for the errors in sound absorption found in Gabard (2013) when using the Myers condition. In contrast, the single-step implicit scheme modes have destabilised and have the wrong sign for $\mathrm{Im}(k)$; this could be due to either a failing of the method or a wrong choice of sign for the square roots in the derivation (see appendix D for a detailed discussion). Both asymptotic methods correctly predict the Pridmore-Brown result.

Figure 6(*a*) shows results for $\omega = 10$, $m = 5$ and $\delta = 1 \times 10^{-3}$, with the addition of modes predicted by the $O(\delta^2)$ asymptotic solution surface mode dispersion relation
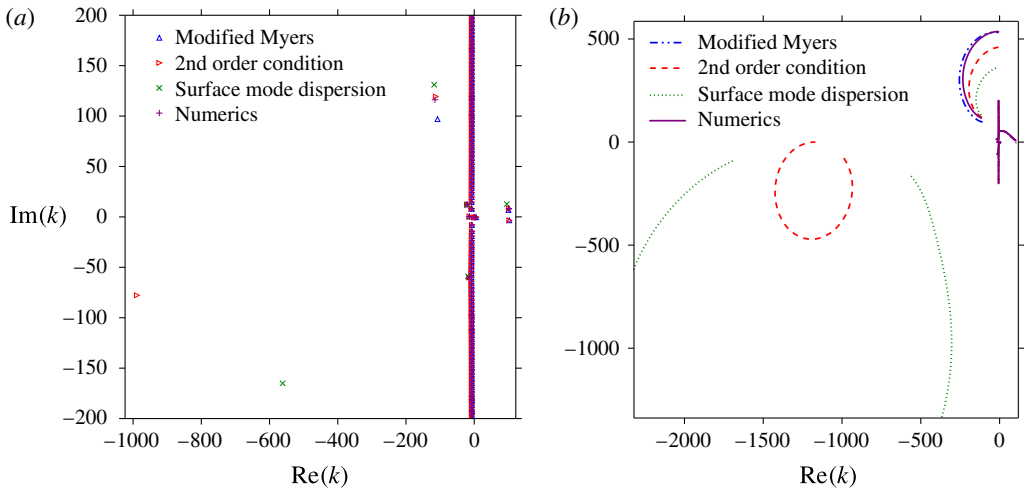
FIGURE 6. (Colour online) (*a*) Surface modes near the origin for $Z_b = 1 - 2.5i$, where here the mass–spring–damper model is not used. (*b*) A larger view of the k-plane, with tracks of surface modes as $\text{Im}(Z_b)$ is increased from -2.5 with $\text{Re}(Z_b) = 1$ held constant. A spurious mode can be seen far from the origin. In both panels the parameters are $\omega = 10$, $m = 5$ and $\delta = 1 \times 10^{-3}$, for a tanh profile with $M = 0.5$.

(6.8). The good agreement between the $O(\delta^2)$ asymptotic solution and its surface mode dispersion relation for the four surface modes near the main spectrum on the right of figure 6(*a*) shows that the reduced model (6.8) is working as intended. Importantly, the two modes in the lower left corner are unique to the $O(\delta^2)$ asymptotic solution and its surface mode approximation, with no counterparts found using either the modified Myers condition or the full numerics. These modes also fall outside the range of validity of the asymptotics, since they do not satisfy $|k| \ll 1/\delta$. Figure 6(*b*) shows the movement of the modes as $\text{Im}(Z_b)$ is increased from -2.5 to sufficiently positive, where the mass–spring–damper liner model is not used. The four surface modes near the main spectrum join, or interact with, the cut-off modes as the impedance is varied. However, the modes in the lower left do not interact with the other modes in any way. These two pieces of information about the modes in the lower left – their irreproducibility by the numerics, and their unphysical isolation from the main spectrum – suggest that they are spurious. Thus, as the surface mode dispersion relation (6.8) has been shown to be a valid approximation of (3.8), we may use it to suggest that the $O(\delta^2)$ asymptotic solution predicts eight spurious surface modes. This may not be as harmful to the predictive power of the model as it seems at first: new modes could only exist (for reasonable ω and m) for k values large enough to bring the $O(\delta^2)$ terms of (3.8) into balance with the $O(\delta)$ or $O(1)$ terms. This would inherently mean moving outside the region of asymptotic validity of the model, and hence a careful use of the new condition should prevent spurious modes being mistakenly deemed important. Indeed, the spurious modes in figure 6 are outside the region of asymptotic validity, given by $|k| \ll 1000$.

7.1. *The unstable hydrodynamic mode*

Surface modes are important for stability analyses. In a laminar boundary layer, linearly unstable surface modes can seed turbulence, which subsequently causes the
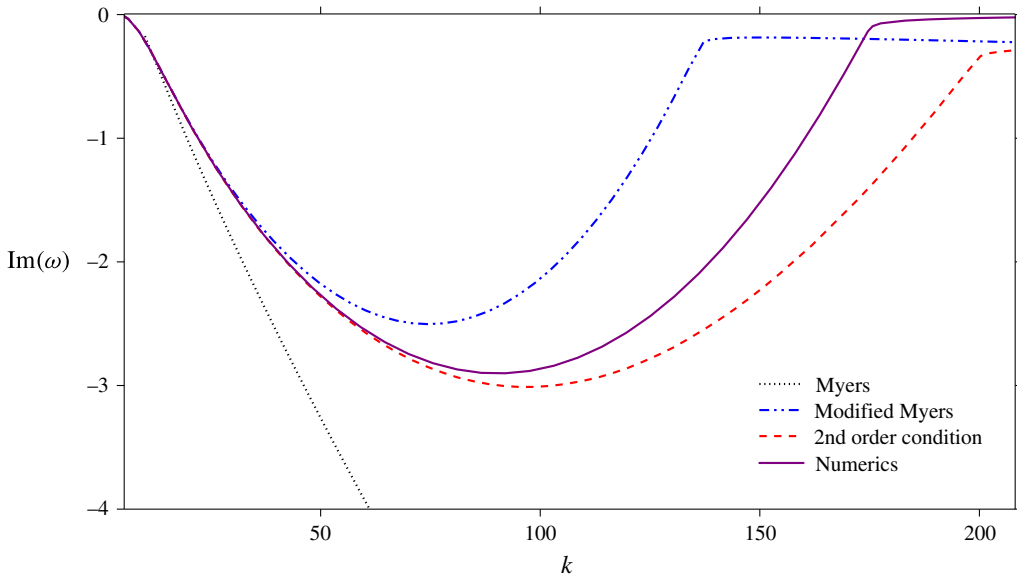
FIGURE 7. (Colour online) The unstable mode growth rate is plotted against real k for parameters $\delta = 2 \times 10^{-3}$, $m = 12$, $M = 0.5$, with a tanh boundary layer profile and a mass–spring–damper impedance, $Z_b(\omega) = R + i\omega d - ib/\omega$, for $R = 3$, $d = 0.15$, $b = 1.15$, as in (7.1).

boundary layer to thicken. Instability waves are also known to be a source of sound radiation (e.g. Tam & Morris 1980), so being better able to predict the linear stability of the boundary layer over a liner is extremely important for aeroacoustic applications where noise suppression is the goal.

The unstable hydrodynamic modes (Rienstra 2003; Brambley & Peake 2006) of the asymptotic boundary conditions (2.7), (2.9) and (3.8) are traced for increasing real k in figure 7, and compared with Pridmore-Brown numerics, where now we are solving for ω given k. The growth rate of the mode is $-\text{Im}(\omega)$. The $O(\delta^2)$ asymptotic solution (dashed) replicates the full numerical solution (solid) accurately for moderate k. In this case, it is a quantitatively better approximation than the modified Myers for $k \lesssim 160$, which would be considered a very large wavenumber for most practical purposes. The $O(\delta^2)$ asymptotic solution retains the regularisation that results from considering a finite-thickness shear layer; that is, applying the condition (3.8) (within its region of asymptotic validity) forms a well-posed system. It is therefore a usefully predictive tool for investigating maximum growth rates and representative wavelengths of the linear instability of an inviscid boundary layer over an impedance lining. For completeness, the Myers boundary condition prediction is plotted in figure 7 (black dotted); its illposedness manifests as an unbounded growth rate. The Pridmore-Brown solution asymptotes to $\text{Im}(\omega) = 0$ as $k \to \infty$ but never becomes stable ($\text{Im}(\omega) > 0$) for any real k. Viscosity controls the restabilisation at small wavelengths (Khamis & Brambley 2015): we would therefore not expect the inviscid numerics nor the inviscid boundary conditions (2.9) and (3.8) to be stable at large real k without the addition of a small amount of viscosity to stabilise the system for large wavenumbers.

8. Conclusion

Analytical modelling of flow over a lining, where the acoustics in a uniform flow may be expressed in terms of Bessel functions and modes found by applying an effective impedance boundary condition, may be improved by using the second-order asymptotic boundary condition derived here, equation (3.8). The model has been shown to predict with greater accuracy both cut-off and cut-on modes, as well as surface modes. When the boundary layer thickness δ is small and the wavenumber and frequency satisfy $k, \omega \ll 1/\delta$, the second-order condition consistently and accurately predicts numerical solutions of the Pridmore-Brown equation, improving on the modified Myers condition (Brambley 2011*b*) and retaining its wellposedness.

For numerics in the frequency domain, the boundary conditions derived here may be easily applied in their general forms, (3.8) and (4.11), or simplified by assuming a specific shear profile; for example, a linear profile leads to expressions (6.2) and (6.4). For sufficiently thin boundary layers, the second-order asymptotic condition allows the accurate prediction of growth rates and characteristic wavelengths of instability. The effect of the shear is modelled more precisely than in previous modifications of the Myers condition, improving predictions of the position of cut-on modes in the k-plane. This should increases the accuracy of attenuation calculations. For thick boundary layers or high wavenumbers/frequencies outside the region of asymptotic validity, the single-step implicit Runge–Kutta boundary condition (4.11) could be carefully used, with the associated caveats kept in mind. It has been evidenced here that the implicit Runge–Kutta condition can produce very accurate predictions of the effective impedance. The scheme performs poorly, however, when predicting the wavenumber and behaviour of surface modes and modes with sharp changes in the boundary layer forced by the shear, owing to its poor resolution of waves in the boundary layer. A higher-order implicit method could solve this problem, but for such a method a closed form of the boundary condition would be overly complicated.

The new second-order asymptotic condition predicts surface modes with a higher degree of accuracy than the modified Myers condition, but also predicts additional spurious surface modes. Asymptotic analysis of the $k/\omega \gg 1$ regime has shown that the new condition predicts a possible 14 surface modes, compared to the six of the modified Myers condition (Brambley 2013) and four of the Myers condition (Rienstra 2003). By comparison with computations, it is suggested that the extra modes predicted by the second-order condition are spurious, and are easily recognised by being far out of the range of asymptotic validity. Analysis of the single-step implicit scheme boundary condition leads to a prediction of six surface modes, matching the prediction of the modified Myers. Also introduced at the second order of the asymptotic expansion is the spurious singularity when $(\omega - Mk)^2 = k^2 + m^2$, near which the first-order condition or implicit Runge–Kutta condition could be used instead.

Impedance eduction techniques, which, broadly speaking, allow the inference of the impedance of a material from its response to different frequencies of sound, are dependent on the quality of the liner model that they employ. The second-order asymptotic condition derived here has more parameters (the δI_j integrals) than previous models, meaning more degrees of freedom with which to achieve a better fit to the data (or, indeed, with which to 'back out' some information about the base flow).

The application of impedance conditions in grazing flow in the time domain is an open question. The Myers condition has been applied in the time domain in many different ways, and is still a topic of current research (e.g. Gabard & Brambley 2014). The use of the modified Myers condition in the time domain has been only tentatively

studied, and application of the new conditions derived here in the time domain would be interesting future work.

The general problem of a liner with grazing flow has many facets which themselves are open problems; including visco-thermal effects which are in the most part neglected in the literature. It is known that viscosity by itself does not regularise the illposedness of the Myers condition (Brambley 2011*a*), but that viscous effects can be necessary to accurately predict experimental results (Renou & Aurégan 2011). The combination of viscous effects and an expansion in the boundary layer thickness is current work (Khamis & Brambley 2015).

Acknowledgement

Appendix A. Details of the asymptotics of the $\tilde{p}$ and $\tilde{v}$ governing equations

We solve (3.4) to second order for the inner solution by expanding the radial velocity as $\tilde{v} = \tilde{v}_0 + \delta \tilde{v}_1 + \delta^2 \tilde{v}_2 + O(\delta^3)$. We match to the outer solution

$$
\begin{aligned}
\tilde{v}_u(1 - \delta y) \;=\; & v_\infty + \delta y \left(\frac{\mu^2}{\mathrm{i}\Omega_u} p_\infty + v_\infty \right) \\
& + \frac{1}{2}\delta^2 y^2 \left[(2 + \mu^2) v_\infty + \frac{\mu^2 + 2m^2}{\mathrm{i}\Omega_u} p_\infty \right] + O(\delta^3)
\end{aligned}
\tag{A 1}
$$

in the limit $y \to \infty$, where for brevity $\Omega_u = \omega - Mk$ and $\mu^2 = k^2 + m^2 - \Omega_u^2$. With $\Omega = \omega - Uk$ and $\sigma_+ = k^2 + m^2$, the leading-order solution is

$$
\tilde{v}_0 = A_0 \Omega + B_0 \Omega \int_0^y \left(1 - \frac{\sigma_+}{\rho \Omega^2} \right) \mathrm{d}y',
\tag{A 2}
$$

which may be written in terms of bounded integrals as

$$
\tilde{v}_0 = A_0 \Omega - B_0 \Omega y \frac{\mu^2}{\Omega_u^2} + B_0 \Omega \frac{\sigma_+}{\Omega_u^2} \int_0^y \left(1 - \frac{\Omega_u^2}{\rho \Omega^2} \right) \mathrm{d}y'.
\tag{A 3}
$$

Upon matching with the leading order of (A 1) as $y \to \infty$, we find $B_0 \equiv 0$ and $A_0 = v_\infty / \Omega_u$. Similarly, at first order,

$$
\tilde{v}_1 = A_1 \Omega + A_0 \Omega y - B_1 \Omega y \frac{\mu^2}{\Omega_u^2} + B_1 \Omega \frac{\sigma_+}{\Omega_u^2} \int_0^y \left(1 - \frac{\Omega_u^2}{\rho \Omega^2} \right) \mathrm{d}y'.
\tag{A 4}
$$

Matching with (A 1) gives $B_1 = \mathrm{i} p_\infty$ and $A_1 = -\mathrm{i}\sigma_+ I_1 p_\infty / \Omega_u^2$, where

$$
I_1 = \int_0^\infty \chi_1(y) \, \mathrm{d}y, \quad \chi_1(y) = 1 - \frac{(\omega - Mk)^2}{\rho(\omega - Uk)^2}.
\tag{A 5a,b}
$$

At second order, we find

$$
\begin{aligned}
\tilde{v}_2 ={}& A_2\Omega - B_2\Omega y\frac{\mu^2}{\Omega_u^2} + B_2\Omega\frac{\sigma_+}{\Omega_u^2}\int_0^y \chi_1\,\mathrm{d}y' + A_1\Omega y - B_1\Omega\int_0^y y\frac{\mu^2}{\Omega_u^2}\,\mathrm{d}y' \\
&+ B_1\Omega\frac{\sigma_+}{\Omega_u^2}\int_0^y\left(\int_0^{y'}\chi_1\,\mathrm{d}y'' - I_1\right)\mathrm{d}y' + B_1\Omega\frac{\sigma_+}{\Omega_u^2}I_1 y + \frac{1}{2}A_0\Omega y^2 \\
&- 2m^2\Omega\left(A_0 - B_1\frac{\mu^2}{\Omega_u^2}\right)\int_0^y\frac{y'}{\rho\Omega^2-\sigma_+}\,\mathrm{d}y' - 2m^2 B_1\Omega\frac{\sigma_+}{\Omega_u^2}\int_0^y\frac{y'}{\rho\Omega^2-\sigma_+}\chi_1\,\mathrm{d}y' \\
&+ A_0\Omega\int_0^1 y'\left(1 + \frac{2m^2}{\rho\Omega^2-\sigma_+}\right)\mathrm{d}y' - A_0\Omega\int_0^y\left(1 - \frac{\sigma_+}{\rho\Omega^2}\right)\int_0^{y'}\rho\Omega^2\,\mathrm{d}y''\,\mathrm{d}y'.
\end{aligned}
\tag{A 6}
$$

In terms of bounded integrals suitable for matching, (A 6) may be rewritten as

$$
\begin{aligned}
\tilde{v}_2 ={}& A_2\Omega - B_2\Omega y\frac{\mu^2}{\Omega_u^2} + B_2\Omega\frac{\sigma_+}{\Omega_u^2}\int_0^y\chi_1\,\mathrm{d}y' + A_1\Omega y - \frac{\mu^2\Omega}{2\Omega_u^2}B_1 y^2 - \frac{m^2\Omega}{\Omega_u^2}B_1 y^2 \\
&+ B_1\Omega\frac{\sigma_+}{\Omega_u^2}\int_0^y\left(\int_0^{y'}\chi_1\,\mathrm{d}y'' - I_1\right)\mathrm{d}y' + B_1\Omega\frac{\sigma_+}{\Omega_u^2}I_1 y + \frac{1}{2}A_0\Omega y^2 + \frac{m^2\Omega}{\mu^2}A_0 y^2 \\
&+ m^2\Omega\left(\frac{2B_1}{\Omega_u^2} - \frac{A_0}{\mu^2}\right)\int_0^y y'\left(1 - \frac{\Omega_u^2-\sigma_+}{\rho\Omega^2-\sigma_+}\right)\mathrm{d}y' + \frac{2m^2\sigma_+}{\Omega_u^2}\frac{\Omega}{\mu^2}B_1\int_0^y\chi_1 y'\,\mathrm{d}y' \\
&- \frac{2m^2\sigma_+}{\Omega_u^2}\frac{\Omega}{\mu^2}B_1\int_0^y\chi_1 y'\left(1 - \frac{\Omega_u^2-\sigma_+}{\rho\Omega^2-\sigma_+}\right)\mathrm{d}y' + A_0\sigma_+\Omega\int_0^y\chi_1\int_0^{y'}\chi_0\,\mathrm{d}y''\,\mathrm{d}y' \\
&- A_0\Omega\mu^2\int_0^y\left(\int_0^{y'}\chi_0\,\mathrm{d}y'' - I_0\right)\mathrm{d}y' - A_0\Omega\mu^2 I_0 y - A_0\sigma_+\Omega\int_0^y y'\chi_1\,\mathrm{d}y' \\
&+ \frac{1}{2}A_0\Omega\mu^2 y^2,
\end{aligned}
\tag{A 7}
$$

where

$$
I_0 = \int_0^\infty \chi_0(y)\,\mathrm{d}y, \quad \chi_0(y) = 1 - \frac{\rho(\omega-Uk)^2}{(\omega-Mk)^2}.
\tag{A 8a,b}
$$

At this order in the $\tilde{v}$ expansion, we introduce spurious singularities at $\mu^2 = 0$ and $\rho\Omega^2 = \sigma_+$. Taking $y \to \infty$ and matching with the outer solution gives

$$
B_2 = \frac{\Omega_u^2}{\mu^2}A_1 + \frac{\sigma_+}{\mu^2}I_1 B_1 - \Omega_u^2 I_0 A_0
\tag{A 9}
$$

and

$$
\begin{aligned}
A_2 ={}& -B_2\Omega\frac{\sigma_+}{\Omega_u^2}I_1 - B_1\frac{\sigma_+}{\Omega_u^2}\int_0^\infty\left(\int_0^y\chi_1\,\mathrm{d}y' - I_1\right)\mathrm{d}y - m^2\left(\frac{2B_1}{\Omega_u^2} - \frac{A_0}{\mu^2}\right)\int_0^y y'\chi_2\,\mathrm{d}y' \\
&- \frac{2m^2\sigma_+}{\Omega_u^2\mu^2}I_3 B_1 + \frac{2m^2\sigma_+}{\Omega_u^2\mu^2}B_1\int_0^\infty y\chi_1\chi_2\,\mathrm{d}y - A_0\sigma_+\int_0^\infty\chi_1\int_0^y\chi_0\,\mathrm{d}y'\,\mathrm{d}y \\
&+ A_0\mu^2\int_0^\infty\left(\int_0^y\chi_0\,\mathrm{d}y' - I_0\right)\mathrm{d}y + A_0\sigma_+ I_3,
\end{aligned}
\tag{A 10}
$$

where

$$I_3 = \int_0^\infty y\chi_1(y)\,\mathrm{d}y \quad\text{and}\quad \chi_2(y) = 1 - \frac{(\omega - Mk)^2 - k^2 - m^2}{\rho(\omega - Uk)^2 - k^2 - m^2}. \tag{A 11a,b}$$

Evaluating $\tilde{v}$ at the wall, $y = 0$, leads to

$$
\begin{aligned}
\tilde{v}(0) &= \frac{\omega}{\Omega_u}\left\{ v_\infty - \frac{\mathrm{i}\sigma_+}{\Omega_u}p_\infty\delta I_1 - \sigma_+\left(\frac{2\mathrm{i}m^2 p_\infty}{\Omega_u\mu^2} - v_\infty\right)\delta^2 I_3 + \sigma_+ v_\infty\delta I_0\delta I_1 \right.\\
&\quad + \frac{\mathrm{i}\sigma_+}{\Omega_u}p_\infty\delta^2 I_3 - \mu^2 v_\infty\delta^2 I_2 - \frac{2\mathrm{i}m^2 p_\infty}{\Omega_u}\delta^2 I_4 - \sigma_+ v_\infty\delta^2 I_5 \\
&\quad \left. + \frac{2\mathrm{i}m^2\sigma_+ p_\infty}{\Omega_u\mu^2}\delta^2 I_6 \right\} + O(\delta^3),
\end{aligned}
\tag{A 12}
$$

where

$$I_4 = \int_0^\infty y\chi_2(y)\,\mathrm{d}y, \quad I_5 = \int_0^\infty \chi_1(y)\int_0^y \chi_0(y')\,\mathrm{d}y'\,\mathrm{d}y, \quad I_6 = \int_0^\infty y\chi_1(y)\chi_2(y)\,\mathrm{d}y. \tag{A 13a$-$c}$$

Equation (A 12) is equivalent to (3.5b) in the main part of the paper.

The corresponding problem for $\tilde{p}$ is solved in the same way, using the governing equation (3.3) and the outer solution (3.2a). The result is given in appendix A of Brambley (2011b) as

$$
\begin{aligned}
\tilde{p}(0) &= p_\infty + \mathrm{i}(\omega - Mk)v_\infty\delta I_0 + p_\infty(k^2 + m^2)\delta I_1\delta I_0 + \mathrm{i}(\omega - Mk)v_\infty\delta^2 I_2 \\
&\quad - (\omega - Mk)^2 p_\infty\delta^2 I_7 - p_\infty(k^2 + m^2)\delta^2 I_3,
\end{aligned}
\tag{A 14}
$$

where

$$I_2 = \int_0^\infty y\chi_0(y)\,\mathrm{d}y \quad\text{and}\quad I_7 = \int_0^\infty \chi_0(y)\int_0^y\left(1 - \frac{k^2 + m^2}{\rho(y')(\omega - U(y')k)^2}\right)\mathrm{d}y'\,\mathrm{d}y. \tag{A 15a,b}$$

The effective impedance is formed by taking the ratio $Z_b = \tilde{p}(0)/\tilde{v}(0)$ and dividing top and bottom by v_∞. This gives $Z_b = f(Z_{eff})$ by virtue of the definition $Z_{eff} = p_\infty/v_\infty$; rearranging for Z_{eff} produces

$$Z_{eff} = \frac{\omega}{\Omega_u}\frac{Z_b + \delta\mathscr{A} + \delta^2\mathscr{B}}{1 + \delta\mathscr{C} + \delta^2\mathscr{D}} + O(\delta^3), \tag{A 16}$$

where

$$
\left.
\begin{aligned}
&\mathscr{A} = -\frac{\mathrm{i}\Omega_u^2}{\omega}I_0, \quad \mathscr{B} = -\frac{\mathrm{i}\Omega_u^2}{\omega}I_2 - Z_b\mu^2 I_2 + \sigma_+ Z_b(I_0 I_1 + I_3 - I_5), \quad \mathscr{C} = \mathrm{i}\sigma_+\frac{\omega Z_b}{\Omega_u^2}I_1, \\
&\mathscr{D} = \frac{\mathrm{i}\sigma_+\omega Z_b}{\Omega_u^2}\left(\frac{2m^2}{\mu^2} - 1\right)I_3 + 2\mathrm{i}m^2\frac{\omega Z_b}{\Omega_u^2}\left(I_4 - \frac{\sigma_+}{\mu^2}I_6\right) + \sigma_+(I_0 I_1 - I_3) - \Omega_u^2 I_7,
\end{aligned}
\right\}
\tag{A 17}
$$

which is equivalent to (3.8).

Appendix B. Asymptotics of the impedance governing equation

Here we derive, asymptotically, two expressions for Z_{eff} from the nonlinear impedance equation (4.1), correct to first and second order in δ, respectively.

In the case of a non-uniform flow, where $U = U(r)$ and $\rho = \rho(r)$, we use (4.3) in (4.1) and substitute for L'_u from (4.4) to arrive at (4.5), which we repeat here for convenience:

$$\frac{1}{(\omega - Mk)}\tilde{L}' = \frac{i}{r}\left[1 - \frac{\rho(\omega - Uk)^2}{(\omega - Mk)^2}\right] + ir\frac{k^2 + \dfrac{m^2}{r^2}}{(\omega - Mk)^2}\left[1 - \frac{(\omega - Mk)^2}{\rho(\omega - Uk)^2}\right]L_u^2$$

$$+ ir\left[1 - \frac{k^2 + \dfrac{m^2}{r^2}}{\rho(\omega - Uk)^2}\right](2L_u\tilde{L} + \tilde{L}^2). \tag{B 1}$$

The first two square brackets on the right-hand side of (B 1) are non-zero only in the thin boundary layer near $r = 1$. This suggests that a power series expansion of $\tilde{L}$ in the boundary layer thickness δ is appropriate, so we write $\tilde{L} = \delta\tilde{L}_1 + \delta^2\tilde{L}_2 + O(\delta^3)$. The last square bracket is multiplied by terms proportional to $\tilde{L}$ and $\tilde{L}^2$, so the order-of-magnitude assumptions are self-consistent. We again rescale to lie within the boundary layer by writing $r = 1 - \delta y$. Expanding (B 1) in terms of y and in powers of δ produces

$$\frac{1}{\Omega_u}(\tilde{L}_1 + \delta\tilde{L}_2)' = -i\chi_0 - i\frac{\sigma_+}{\Omega_u^2}L_u(0)^2\chi_1 - \delta\left\{iy\chi_0 + iy\frac{\sigma_-}{\Omega_u^2}L_u(0)^2\chi_1\right.$$

$$\left. - 2iy\frac{\sigma_+}{\Omega_u^2}L_u(0)L'_u(0)\chi_1 + 2i\left(1 - \frac{\sigma_+}{\rho\Omega^2}\right)L_u(0)\tilde{L}_1\right\}, \tag{B 2}$$

where $\sigma_\pm = m^2 \pm k^2$, $\Omega(y) = \omega - U(y)k$, $\Omega_u = \omega - Mk$, and the χ_j are defined as in (3.7). Our boundary conditions are $\tilde{L}_j \to 0$ as $y \to \infty$ for $j = 1, 2$. In (B 2) the Taylor expansion of L_u about the lined wall, $L_u(y) = L_u(0) - \delta y L'_u(0) + O(\delta^2)$, is used. We note that in this section all arguments are now in terms of y unless explicitly stated; a prime represents a derivative with respect to y, and an argument of $y = 0$ relates to a value at the wall, where $r = 1$.

We may integrate the leading-order terms in (B 2) to find an expression for $\tilde{L}_1$,

$$\tilde{L}_1 = i\Omega_u\left[I_0 - \int_0^y \chi_0(z)\,dz + \frac{\sigma_+}{\Omega_u^2}L_u^2(0)\left(I_1 - \int_0^y \chi_1(z)\,dz\right)\right], \tag{B 3}$$

where the integration constants I_j are defined as in (3.6). This ensures that $\tilde{L}_1 \to 0$ as $y \to \infty$, such that, as we move into the main body of the duct, where the flow is uniform, our L value tends to its uniform flow value L_u. Evaluating (B 3) at $y = 0$ causes the integrals to vanish, and thus we find an expression for L at the wall, correct to first order in δ:

$$L(0) = L_u(0) + i\Omega_u\delta\left[I_0 + I_1\frac{\sigma_+}{\Omega_u^2}L_u^2(0)\right] + O(\delta^2). \tag{B 4}$$

From (4.2), no slip at the boundary implies $L(0) = \omega Z_b/\Omega_u$. Similarly, a uniform slipping flow implies $L_u(0) = Z_{eff}$. At leading order, then, (B 4) becomes

$$Z_{eff} = \frac{\omega}{\Omega_u} Z_b + O(\delta), \tag{B 5}$$

which is the Myers effective impedance (2.7), as expected (Myers 1980). If we make the approximation $L_u^2(0) = Z_b Z_{eff}/(1 - Mk/\omega) + O(\delta)$, we can rearrange (B 4) at first order to find

$$Z_{eff} = \frac{\omega}{\Omega_u} \frac{Z_b - \dfrac{i}{\omega} \Omega_u^2 \delta I_0}{1 + i\sigma_+ \dfrac{\omega Z_b}{\Omega_u^2} \delta I_1} + O(\delta^2), \tag{B 6}$$

which is the modified Myers effective impedance (2.9), as derived using matched asymptotic expansions of $\tilde{p}$ in Brambley (2011b).

Continuing, the first-order terms in (B 2) may be examined to find the second-order correction terms. Upon integration,

$$\begin{aligned}
\tilde{L}_2 = i\Omega_u \Bigg\{ & I_2 - \int_0^y z\chi_0(z) \, dz + \Gamma L_u(0) \left(I_3 - \int_0^y z\chi_1(z) \, dz \right) \\
& + 2L_u(0) \left(I_8 - \int_0^y \tilde{L}_1(z) \left[1 - \frac{\sigma_+}{\rho(z)\Omega(z)^2} \right] dz \right) \Bigg\},
\end{aligned} \tag{B 7}$$

where

$$\Gamma = \frac{\sigma_-}{\Omega_u^2} L_u(0) - 2i \frac{\sigma_+}{\Omega_u} \left[1 - \left(1 - \frac{\sigma_+}{\Omega_u^2} \right) L_u(0)^2 \right] \tag{B 8}$$

and the new integration constant, I_8, is defined by

$$I_8 = \int_0^\infty \tilde{L}_1 \left[1 - \frac{\sigma_+}{\rho\Omega^2} \right] dy. \tag{B 9}$$

As before, this ensures that $\tilde{L}_2 \to 0$ as $y \to \infty$ such that we find the correct behaviour in the uniform core of the duct. Using (B 3) and (B 7) in (4.3) we have, at the boundary,

$$L(0) = L_u(0) + i\Omega_u \left(\delta \left[I_0 + I_1 \frac{\sigma_+}{\Omega_u^2} L_u^2(0) \right] + \delta^2 \left[I_2 + \Gamma L_u(0) I_3 + 2L_u(0) I_8 \right] \right) + O(\delta^3). \tag{B 10}$$

By rearranging (B 10) we find the effective impedance,

$$Z_{eff} = \frac{\omega}{\Omega_u} \frac{Z_b - \dfrac{i}{\omega} \Omega_u^2 (\delta I_0 + \delta^2 I_2)}{1 + i\delta \dfrac{\sigma_+}{\Omega_u} L_u(0) I_1 + i\Omega_u \delta^2 (\Gamma I_3 + 2I_8)} + O(\delta^3), \tag{B 11}$$

where the values of $L_u(0)$ in the denominator, in the Γ term and in the I_8 integral must be approximated. Herein lies a key issue with this method: the nonlinear L_u terms force approximations to be made for which there is no guiding *modus operandi*.

In the matched asymptotic expansions derivation which leads to the condition (3.8), no such Z_{eff}^2 splittings have to be made; the linear form falls naturally out of the mathematics. Different asymptotic forms of (B 11) may be found by using different approximations, and it transpires that the behaviour of the boundary condition (B 11) is heavily dependent on the chosen form. While (3.8) and (B 11) are asymptotically equivalent, it is difficult to see from (B 11) any reason to choose the approximation leading to (3.8), although other approximations seem to give worse results than (3.8).

We conclude by remarking that, although a unique, useful second-order condition does not fall easily out of the impedance governing equation, the derivation of the first-order modified Myers condition is cleaner than that of Brambley (2011*b*).

Appendix C. Surface mode asymptotics of I_j integrals

The integrals I_j are approximated in the $k/\omega \gg 1$ limit as

$$
\left.
\begin{aligned}
\delta I_0 &= \frac{1}{(\omega - Mk)^2}(\omega^2 \delta_{mass} - 2Mk\omega\delta_{mom} + M^2 k^2 \delta_{ke}), \quad \delta I_1 \sim \delta_s \frac{Mk}{\omega}, \\
\delta^2 I_2 &= \frac{1}{(\omega - Mk)^2}(\omega^2 \tilde{\delta}_{mass}^2 - 2Mk\omega\tilde{\delta}_{mom}^2 + M^2 k^2 \tilde{\delta}_{ke}^2), \\
\delta^2 I_3 &\sim \delta^2 \left[\frac{3}{2} + \ln\left(\frac{\omega/k}{\omega/k - M} \right) \right], \\
\delta^2 I_4 &\sim \int_0^1 (1-r)\left(1 - \frac{M^2 - 1}{\rho U^2 - 1} \right) dr + \frac{\omega}{k} \int_0^1 \frac{2(1-r)}{\rho U^2 - 1}\left(M - \frac{\rho U(M^2 - 1)}{\rho U^2 - 1} \right) dr, \\
\delta^2 I_5 &\sim \delta^2 \left[\frac{\frac{19}{12}M^2 k^2 - \frac{13}{3}Mk\omega}{(\omega - Mk)^2} + \ln\left(\frac{\omega/k}{\omega/k - M} \right) \right], \\
\delta^2 I_6 &\sim \delta^2 \left[\frac{1}{2} + M^2 + M^2 \ln\left(\frac{\omega/k}{\omega/k - M} \right) \right. \\
&\qquad \left. + \frac{1 - M^4}{2M^2} \ln\left(1 - \frac{Mk(Mk - 2\omega)}{(\omega - Mk)^2 - k^2 - m^2} \right) \right], \\
\delta^2 I_7 &\sim \frac{\delta_s(k^2 + m^2)}{Mk\omega(\omega - Mk)^2}(\omega^2 \delta_{mass} - 2Mk\omega\delta_{mom} + M^2 k^2 \delta_{ke}),
\end{aligned}
\right\}
\tag{C 1}
$$

where I_0 and I_2 are exact, and

$$
\left.
\begin{aligned}
\delta_s &= \frac{-M}{\rho(1)U'(1)}, \quad \delta_{mass} = \int_0^1 (1 - \rho)\, dr, \quad \delta_{mom} = \int_0^1 1 - \frac{\rho U}{M}\, dr, \\
\delta_{ke} &= \int_0^1 1 - \frac{\rho U^2}{M^2}\, dr, \quad \tilde{\delta}_{mass}^2 = \int_0^1 (1-r)(1 - \rho)\, dr, \\
\tilde{\delta}_{mom}^2 &= \int_0^1 (1-r)\left(1 - \frac{\rho U}{M} \right) dr, \quad \tilde{\delta}_{ke}^2 = \int_0^1 (1-r)\left(1 - \frac{\rho U^2}{M^2} \right) dr
\end{aligned}
\right\}
\tag{C 2}
$$

are measures of boundary layer thickness.

Appendix D. The implicit scheme

The second-order trapezoidal single-step implicit scheme is the highest-order such scheme for which a closed-form solution can be written. The fundamental difference equation for the differential equation $y' = f(x, y)$ is

$$y_{n+1} = y_n + \frac{h}{2}(f(x_n, y_n) + f(x_{n+1}, y_{n+1})), \tag{D 1}$$

which may be written as

$$y_{n+1} = y_n + \frac{h}{2}(k_1 + k_2), \tag{D 2}$$

where

$$k_1 = f(x_n, y_n), \quad k_2 = f\left(x_n + h, y_n + \frac{h}{2}k_1 + \frac{h}{2}k_2\right). \tag{D 3a,b}$$

We use this scheme to solve (4.1) and (4.4), which we rewrite together here in the form

$$L' = A_j(r) + B_j(r)L^2, \tag{D 4}$$

for $j = 1, 2$, with

$$\left.\begin{array}{ll} A_1(r) = -\dfrac{\mathrm{i}}{r}\dfrac{\rho(\omega - Uk)^2}{\omega - Mk}, & B_1(r) = \mathrm{i}r(\omega - Mk)\left(1 - \dfrac{k^2 + m^2/r^2}{\rho\Omega^2}\right), \\[3mm] A_2(r) = -\dfrac{\mathrm{i}}{r}(\omega - Mk), & B_2(r) = \mathrm{i}r(\omega - Mk)\left(1 - \dfrac{k^2 + m^2/r^2}{(\omega - Mk)^2}\right). \end{array}\right\} \tag{D 5}$$

Equation (D 4) with $j = 1$ is the impedance governing equation for a sheared flow (our boundary layer), while for $j = 2$ it is the corresponding equation for a uniform flow (our imagined slipping flow with no sheared boundary layer).

This scheme actually performs two steps, one for each boundary layer, sheared and uniform. Starting from the boundary $r = 1$ with the known impedance Z_b, we step backwards a distance δ through the sheared boundary layer (equation (D 4) with $j = 1$):

$$k_1 = A_1(1) + B_1(1)X_0^2, \tag{D 6a}$$

$$\begin{aligned} k_{2\pm} = {} & \frac{2}{\delta^2 B_1(1 - \delta)} + 2\frac{X_0}{\delta} - k_1 \\ & \pm \sqrt{\left(\frac{2}{\delta^2 B_1(1 - \delta)} + 2\frac{X_0}{\delta} - k_1\right)^2 - \frac{4}{\delta^2}\left(\frac{A_1(1 - \delta)}{B_1(1 - \delta)} + \left(X_0 - \frac{1}{2}\delta k_1\right)^2\right)}, \end{aligned} \tag{D 6b}$$

leading to

$$X_{1\pm} = X_0 - \tfrac{1}{2}\delta(k_1 + k_{2\pm}). \tag{D 7}$$

The quantity $X_0 = \omega Z_b/(\omega - Mk)$ is $L(1)$ as defined in (4.2), and gives the recovery of the Myers condition in the limit $\delta \to 0$. There are two possible solutions from the

square root; however, it is possible to disregard one by considering the small-δ limit. From (D 6b), $k_{2\pm}$ may be rewritten

$$k_{2\pm} = Y \pm Y\sqrt{1 + W}, \tag{D 8}$$

where

$$Y = \frac{2}{\delta^2 B_1(1-\delta)} + 2\frac{X_0}{\delta} - k_1, \quad W = -\frac{4}{\delta^2 Y^2}\left(\frac{A_1(1-\delta)}{B_1(1-\delta)} + (X_0 - \delta k_1/2)^2\right). \tag{D 9a,b}$$

Since Y is $O(1/\delta^2)$, the term inside the square root in (D 8) may be Taylor-expanded as $\sqrt{1 + \delta^2 W} \sim 1 + \delta^2 W/2 + O(\delta^4)$. Taking the positive root leads to $k_{2+} = O(1/\delta^2)$, while taking the negative root gives $k_{2-} = O(1)$. Considering (D 7), the single implicit Runge–Kutta step would produce an $O(1/\delta)$ change between the quantities X_1 and X_0 if k_{2+} was chosen, and an $O(\delta)$ change if k_{2-} was chosen. Over a small distance we expect a stable solution to change by a small amount; thus, we disregard the positive root and write $X_{1\pm} \equiv X_1$. Note, this assumption may break down if $\delta^2 W$ is not a small quantity, or if a mode oscillates rapidly within the boundary layer.

When computing the value of k_2, we rewrite (D 8) to eliminate the possibility of rounding errors for small W. The square root may be expanded as a binomial series when $|W| < 1$,

$$(1 + W)^{1/2} = \sum_{n=0}^{\infty} \binom{\frac{1}{2}}{n} W^n. \tag{D 10}$$

The leading coefficient of (D 10) is unity, which, when multiplied by the Y outside the root, cancels with the first Y term in (D 8) when the correct negative root is taken (by the scaling argument above). The remaining terms in the series, $n \in [1, \infty)$, may be approximated by the Padé approximant $r(z) = p(z)/q(z)$ (for polynomials p, q) with the zeroth-order coefficient of $p(z)$ set to zero. Then, $k_2 = -Yp(W)/q(W)$. If $|W| \geqslant 1$, the explicit square root form (D 8) may be used.

Next, we step forward from the edge of the boundary layer at $r = 1 - \delta$ through the imagined uniform boundary layer ((D 4) with $j = 2$) to the boundary, where the impedance is the effective impedance Z_{eff}. The quantity X_1 serves as our initial condition, and generates a further two solutions:

$$\tilde{k}_1 = A_2(1-\delta) + B_2(1-\delta)X_1^2, \tag{D 11a}$$

$$\tilde{k}_{2\pm} = \tilde{Y} \pm \tilde{Y}\sqrt{1 + \tilde{W}}, \tag{D 11b}$$

where

$$\tilde{Y} = \frac{2}{\delta^2 B_2(1)} - 2\frac{X_1}{\delta} - \tilde{k}_1, \quad \tilde{W} = -\frac{4}{\delta^2 \tilde{Y}^2}\left(\frac{A_2(1)}{B_2(1)} + \left(X_1 + \frac{1}{2}\delta\tilde{k}_1\right)^2\right), \tag{D 12a,b}$$

and where we again take the negative root of $\tilde{k}_{2\pm}$ in (D 11b), writing $\tilde{k}_{2\pm} \equiv \tilde{k}_2$. The computation of $\tilde{k}_2$ may again be done via Padé approximation if $|\tilde{W}| < 1$. Since we have a binomial series with index $1/2$, the same polynomials $p(z)$ and $q(z)$ from above may be used, and evaluated at the new argument $\tilde{W}$. We arrive at a single value for Z_{eff},

$$Z_{eff} = X_1 + \tfrac{1}{2}\delta(\tilde{k}_1 + \tilde{k}_2), \tag{D 13}$$

which is the result in the main part of the paper.

REFERENCES

AURÉGAN, Y. & LEROUX, M. 2008 Experimental evidence of an instability over an impedance wall in a duct with flow. *J. Sound Vib.* **317**, 432–439.

BERS, A. 1983 Space–time evolution of plasma instabilities – absolute and convective. In *Basic Plasma Physics* (ed. A. A. Galeev & R. N. Sudan), Handbook of Plasma Physics, vol. 1, pp. 451–517. North-Holland.

BOYER, G., PIOT, E. & BRAZIER, J.-P. 2011 Theoretical investigation of hydrodynamic surface mode in a lined duct with sheared flow and comparison with experiment. *J. Sound Vib.* **330**, 1793–1809.

BRAMBLEY, E. J. 2009 Fundamental problems with the model of uniform flow over acoustic linings. *J. Sound Vib.* **322**, 1026–1037.

BRAMBLEY, E. J. 2011a Acoustic implications of a thin viscous boundary layer over a compliant surface or permeable liner. *J. Fluid Mech.* **678**, 348–378.

BRAMBLEY, E. J. 2011b Well-posed boundary condition for acoustic liners in straight ducts with flow. *AIAA J.* **49** (6), 1272–1282.

BRAMBLEY, E. J. 2013 Surface modes in sheared boundary layers over impedance linings. *J. Sound Vib.* **332**, 3750–3767.

BRAMBLEY, E. J., DARAU, M. & RIENSTRA, S. W. 2012 The critical layer in linear-shear boundary layers over acoustic linings. *J. Fluid Mech.* **710**, 545–568.

BRAMBLEY, E. J. & PEAKE, N. 2006 Classification of aeroacoustically relevant surface modes in cylindrical lined ducts. *Wave Motion* **43**, 301–310.

BRAMBLEY, E. J. & PEAKE, N. 2008 Stability and acoustic scattering in a cylindrical thin shell containing compressible mean flow. *J. Fluid Mech.* **602**, 403–426.

BRIGGS, R. J. 1964 *Electron-Stream Interaction with Plasmas*. MIT Press.

EVERSMAN, W. & BECKEMEYER, R. J. 1972 Transmission of sound in ducts with thin shear layer – convergence to the uniform flow case. *J. Acoust. Soc. Am.* **52** (1B), 216–220.

GABARD, G. 2013 A comparison of impedance boundary conditions for flow acoustics. *J. Sound Vib.* **332** (4), 714–724.

GABARD, G. & BRAMBLEY, E. J. 2014 A full discrete dispersion analysis of time-domain simulations of acoustic liners with flow. *J. Comput. Phys.* **273**, 310–326.

HAIRER, E., NØRSETT, S. P. & WANNER, G. 1993 *Solving Ordinary Differential Equations I: Nonstiff Problems*. Springer.

INGARD, U. 1959 Influence of fluid motion past a plane boundary on sound reflection, absorption, and transmission. *J. Acoust. Soc. Am.* **31**, 1035–1036.

JOUBERT, L. 2010 Asymptotic approach for the mathematical and numerical analysis of the acoustic propagation in a strong shear flow. PhD thesis, École Polytechnique, Paris.

KHAMIS, D. & BRAMBLEY, E. J. 2015 The effective impedance of a finite-thickness viscothermal boundary layer over an acoustic lining. In *21st AIAA/CEAS Aeroacoustics Conference and Exhibit*, American Institute of Aeronautics and Astronautics.

KOCH, W. & MOEHRING, W. 1983 Eigensolutions for liners in uniform mean flow ducts. *AIAA J.* **21** (2), 200–213.

MARX, D., AURÉGAN, Y., BAILLIET, H. & VALIÉRE, J.-C. 2010 PIV and LDV evidence of hydrodynamic instability over a liner in a duct with flow. *J. Sound Vib.* **329**, 3798–3812.

MCALPINE, A., ASTLEY, R. J., HII, V. J. T., BAKER, N. J. & KEMPTON, A. J. 2006 Acoustic scattering by an axially-segmented turbofan inlet duct liner at supersonic fan speeds. *J. Sound Vib.* **294** (4–5), 780–806.

MYERS, M. K. 1980 On the acoustic boundary condition in the presence of flow. *J. Sound Vib.* **71** (3), 429–434.

MYERS, M. K. & CHUANG, S. L. 1984 Uniform asymptotic approximations for duct acoustic modes in a thin boundary-layer flow. *AIAA J.* **22** (9), 1234–1241.

PIERCE, A. D. 1994 *Acoustics*, 3rd edn. Acoustical Society of America.

PRIDMORE-BROWN, D. C. 1958 Sound propagation in a fluid flowing through an attenuating duct. *J. Fluid Mech.* **4** (4), 393–406.

RENOU, Y. & AURÉGAN, Y. 2010 On a modified Myers boundary condition to match lined wall impedance deduced from several experimental methods in presence of a grazing flow. In *16th AIAA/CEAS Aeroacoustics Conference*, American Institute of Aeronautics and Astronautics.

RENOU, Y. & AURÉGAN, Y. 2011 Failure of the Ingard–Myers boundary condition for a lined duct: an experimental investigation. *J. Acoust. Soc. Am.* **130** (1), 52–60.

RIENSTRA, S. W. 2003 A classification of duct modes based on surface waves. *Wave Motion* **37** (2), 119–135.

RIENSTRA, S. W. & DARAU, M. 2011 Boundary-layer thickness effects of the hydrodynamic instability along an impedance wall. *J. Fluid Mech.* **671**, 559–573.

RIENSTRA, S. W. & VILENSKI, G. G. 2008 Spatial instability of boundary layer along impedance wall. In *14th AIAA/CEAS Aeroacoustics Conference (29th AIAA Aeroacoustics Conference)*, American Institute of Aeronautics and Astronautics.

TAM, C. K. W. & MORRIS, P. J. 1980 The radiation of sound by the instability waves of a compressible plane turbulent shear layer. *J. Fluid Mech.* **98** (2), 349–381.

TESTER, B. J. 1973a Some aspects of 'sound' attenuation in lined ducts containing inviscid mean flows with boundary layers. *J. Sound Vib.* **28**, 217–245.

TESTER, B. J. 1973b The propagation and attenuation of sound in lined ducts containing uniform or plug flow. *J. Sound Vib.* **28** (2), 151–203.

VILENKSI, G. G. & RIENSTRA, S. W. 2007 On hydrodynamic and acoustic modes in a ducted shear flow with wall lining. *J. Fluid Mech.* **583**, 45–70.